NBSIR 77-1404

Control of Mobile-Ion Contamination in Oxidation Ambients for MOS Device Processing

Santos Mayo, Richard Y. Koyama, and Thomas F. Leedy

Electronic Technology Division
Institute for Applied Technology
National Bureau of Standards
Washington, D.C. 20234

January 1978

Final

NBSIR 77-1404

CONTROL OF MOBILE-ION CONTAMINATION IN OXIDATION AMBIENTS FOR MOS DEVICE PROCESSING

Santos Mayo, Richard Y. Koyama, and Thomas F. Leedy

Electronic Technology Division
Institute for Applied Technology
National Bureau of Standards
Washington, D.C. 20234

January 1978

Final

U.S. DEPARTMENT OF COMMERCE, Juanita M. Kreps, *Secretary*

Dr. Sidney Harman, *Under Secretary*

Jordan J. Baruch, *Assistant Secretary for Science and Technology*

NATIONAL BUREAU OF STANDARDS, Ernest Ambler, *Acting Director*

TABLE OF CONTENTS

LIST OF FIGURES

Control of Mobile-Ion Contamination in Oxidation Ambients for MOS Processing

Santos Mayo, Richard Y. Koyama, and Thomas F. Leedy
Institute for Applied Technology
National Bureau of Standards
Washington, D. C.   20234

Abstract

An alternative method for controlling the mobile-ion contamination in the oxidation ambients for MOS device processing is explored. Mobile-ion contamination in silicon dioxide films thermally grown in dry oxygen at 1000°C on silicon substrates has been studied by use of a double-wall fused-silica oxidation tube. The space between the tubes was alternatively filled with chlorine, room air, or sodium hydroxide gas to determine if a correlation exists between the presence of these substances in the jacket and the mobile-ion density in the oxide films. MOS capacitors were prepared on these films and mobile-ion densities were measured using conventional C-V techniques. The ion densities ranged from 10^{13} to 10^{10} cm^{-2} as a function of the jacket atmosphere. These preliminary results suggest that there is a correlation between the presence of cleaning or contaminating agents in the jacket and the mobile-ion density in the oxide films. Both cleaning and contaminating actions occur through the tube wall.

Key words: Double-wall oxidation tube; dry oxidation; mobile-ion contamination; MOS device processing; MOS devices; oxidation ambient control; oxide growth; semiconductor device processing; silicon dioxide; thermal silicon dioxide films.

1.   Introduction

Studies of the electrical properties of thin oxide films used in metal-oxide-semiconductor (MOS) structures have established that mobile-ion contamination in these oxide films causes instabilities of microelectronic devices.[1] Although the properties of the silicon dioxide film and its interfaces at the silicon and metal are not fully understood,[2] and more systematic experimental observation is required, it is generally agreed that alkali contamination of these films should be avoided in order to produce high quality MOS devices.[3] Considerable efforts have been made to detect and neutralize, or eliminate, such contamination during process steps required for device fabrication. Extreme cleanliness during process operations has been recommended, and the use of ultra-pure low mobile-ion chemicals has been explored.[4,5] The use of thin

passivating layers of phosphosilicate glass or silicon nitride on sili-
con dioxide films has been reported,[6],[7] and the addition of small quan-
tities (a few mole percent) of chlorine or hydrogen chloride into the
oxidation atmosphere[8-10] has been shown to facilitate the growth of high
quality thermal silicon dioxide films.

The initial purpose of this task was to develop a measurement tech-
nique which could be used to determine directly the density of sodium in
oxidation atmospheres used for the growth of thermal oxide films on sili-
con. Ideally, a technique for *in situ* measurement of trace contamina-
tion in furnace atmospheres would meet the following conditions: 1) the
measuring system should be sensitive enough to detect impurity densities
in the range of interest for semiconductor applications and 2) the equi-
librium of the furnace atmosphere should be kept unperturbed during the
measurements; for example, introduction of probes into the oxidation
tube or the extraction of atmospheric samples should be avoided. In or-
der to meet these requirements, a laser-induced resonance fluorescence
technique was developed. This technique, which is sensitive to sodium
in an atomic state only, was used to detect sodium in an open fused-
silica oxidation tube operated at 1000°C. The minimum detectable sodium
density was estimated to be approximately 5×10^5 atoms/cm^3. A copy of
the paper which reported the details of this work[11] is included as Appen-
dix 1. The results obtained through this technique led to the conclu-
sion that atomic sodium is not the most abundant species in oxidation
atmospheres contained in fused-silica tubes. Molecular sodium compounds
appear to play an important role in the contamination of such atmo-
spheres.

In view of the above conclusion, a thermodynamic study was made to
evaluate the equilibrium sodium species in oxidation atmospheres con-
tained in both fused silica and silicon tubes operated at 1000°C. Dur-
ing thermal oxidation of silicon, impurities contained in the substrate
or in the oxidation atmosphere come in contact with the growing oxide
film and may become incorporated into it. Contamination of the oxida-
tion ambient may result from impurities in the tube bulk incorporated
during its fabrication process,[12-14] and from contaminants which diffuse
through the tube wall into the oxidation chamber.[15] It was assumed that
the source of sodium contamination in oxidation atmospheres was the tube
wall. Commercially available transparent fused-silica tubes contain
about 10 ppm sodium[12],[13] while silicon tubes contain about 10 ppb sodi-
um.[14] Sodium in such tubes is assumed to be included as a solid solu-
tion of sodium metasilicate in the tube matrix ($Na_2O.SiO_2(c)$ in $SiO_2(c)$).
The thermodynamics of sodium vaporization from sodium silicate-silica
glasses has been previously studied in the temperature range of 1200 to
2000 K where the equilibrium constant of the reaction $Na_2O.SiO_2(c)$ in
$SiO_2(c) \rightarrow 2Na(g) + \frac{1}{2}O_2(g) + SiO_2(c)$ has been measured.[16] Using these
results, reactions occurring at 1300 K on the tube wall were analyzed
when oxygen, water, chlorine, or hydrogen are present in the tube atmo-
sphere. Copies of the papers which report the results of these calcula-
tions[17],[18] are included as Appendices 2 and 3. These calculations show
that the presence of water in the oxidation ambient produces a rapid in-

2

crease of the sodium number density from the 10^7 cm^{-3} range correspond-
ing to dry oxidation to about two orders of magnitude higher for water
concentration of a few ppm. Also, the relevant reactions taking place
during oxidation tube cleaning were thermodynamically analyzed. Empiri-
cally, it is known that the use of chlorine or hydrogen chloride for *in
situ* cleaning of the oxidation tube in processing facilities is needed
to grow oxide films with low mobile-ion content. Periodically, tubes
are flushed for several hours with 5- to 10-percent hydrogen chloride
diluted in an inert carrier gas. The calculations show that during
cleaning the equilibrium sodium density increases by several orders of
magnitude above the sodium level in the normal oxidation atmosphere.
This cleaning produces a sodium-depleted layer at the tube wall adequate
for growing clean oxide films.

Sodium diffuses easily in the tube bulk [diffusion coefficient in
silicon dioxide: 2×10^{-6} cm^2/s][19] to the tube wall surface and replen-
ishes the layer depleted by cleaning, thus necessitating periodic clean-
ing. Contaminants from the furnace heating elements, the refractories,
and the room air continually replenish and add to the sodium contami-
nation in the tube wall. If the tube wall were essentially depleted of
sodium and if external sources of sodium were eliminated for replenish-
ing the tube wall, the oxidation ambient should contribute little mobile-
ion contamination during MOS device processing. These arguments suggest
the use of a double-wall oxidation tube containing chlorine gas between
the inner and outer walls to provide a reactive sink and a barrier for
alkali contamination.

This report summarizes preliminary data on this alternative method
for the preparation of electrically stable thermal oxide films grown at
1000°C without specifically introducing any cleaning or passivating
agents into the oxidation atmosphere.

2. The Experiment

Commercially available transparent fused-silica tubes of appropri-
ate diameter were used to build a double-wall oxidation chamber with a 7-
mm wall separation as shown in figure 1. This tube was operated at
1000°C in a three-zone resistance-heated furnace. At the tube ends, the
inner and outer units were fused together to form a jacket around the
oxidation chamber; no furnace liner was used. This configuration is
similar to a single-wall oxidation tube using a fused-silica liner except
for the joining at both ends. The tube was not cleaned prior to instal-
lation in the furnace. The oxidation tube temperature was constantly
maintained at 1000 ± 2°C. Except for short periods during *in situ* nitro-
gen anneal, the inner oxidation chamber was continuously filled with
electronic grade dry oxygen flowing at a rate of 4 cm^3/s. Although this
oxidation is nominally referred to as dry oxidation, it cannot strictly
be considered so. The commercial electronic grade oxygen used contains
about 5 ppm water and 20 ppm hydrocarbons measured as methane.[20] At
oxidation temperature these hydrocarbons decompose producing additional
water in the oxidation ambient. Moreover, it has been pointed out that
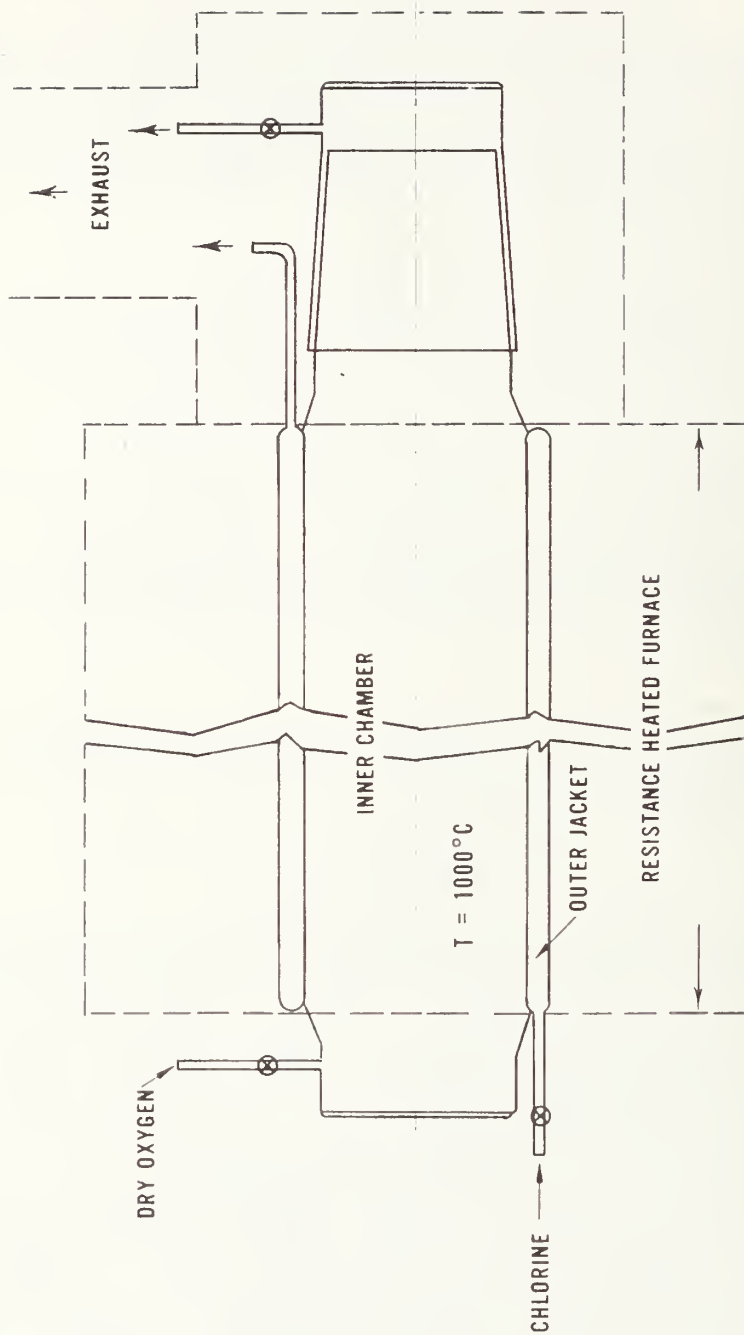
3

Figure 1. Double-wall transparent fused-silica tube used to grow silicon dioxide films. The inner chamber contains the oxidation atmosphere that is fully surrounded by the outer jacket. Chlorine, room air, or sodium hydroxide atmospheres are alternatively established in the jacket for different oxide film growth. The temperature profile in the oxidation chamber shows a central plateau extending about a third of the tube length with ± 1°C variation. The temperature at the furnace center is 1000°C.

at 1000°C, water from the room air around the furnace can permeate through the 1-mm thick fused-silica oxidation tube wall. Assuming 30-percent relative humidity in the room air at 25°C, the number of water molecules[21] permeating through the tube wall is of the order of 10^{10} $cm^{-2} \cdot s^{-1}$. It has been shown that small amounts of water (ppm) in oxygen increase the silicon oxidation rate.[22-24] The chlorine barrier around the oxidation chamber constitutes a sink for water permeating through the tube wall, thus reducing the inclusion of water from room air humidity into the oxidation ambient. The jacket space between the inner and outer tubes was filled with either chlorine (99.9 percent), atmospheric room air, or dilute sodium hydroxide in nitrogen carrier gas, depending upon the desired condition while oxide films were grown in the excitation chamber. While chlorine was used, a porous quartz-wool plug was inserted into the exhaust port of the jacket to minimize chlorine loss to the furnace scavenger. This plug was removed during periods when room air was allowed to backstream into the jacket. The change in jacket atmosphere from air to chlorine could be made in a short interval, while the change from chlorine to air takes a much longer period until the residual chlorine in the jacket is exhausted. In the final stages of the experiment, external contamination was introduced into the jacket by passing nitrogen through a one-percent sodium hydroxide solution at room temperature; the gas was allowed to flow through the jacket by removing the plug from the exhaust.

MOS capacitors were used as test structures to determine the mobile ion content in 100-nm thick, thermal oxide films grown on 5-cm diameter (100) n-type silicon substrates with resistivity in the range from 5 to 10 $\Omega \cdot cm$. The silicon wafers (with one face polished, the other lapped and etched) were cleaned with conventional hydrogen peroxide-ammonia and hydrogen peroxide-acid solutions, rinsed in 18 M$\Omega \cdot cm$ deionized water and spin-dried in nitrogen.[25] After dry oxidation at 1000°C for 212 min, the wafers were annealed *in situ* for 30 min in dry nitrogen.

Metallization by electron-gun evaporation of a 0.5-µm aluminum layer on the oxide film immediately followed the annealing step. Photolithographic techniques were used to define the gate area.* The substrate contact was made by evaporation of a 0.2-µm gold (with 0.6-percent antimony) layer on the entire back side. Finally, the capacitor was annealed at 500°C for 30 min in dry nitrogen. Processing steps such as wafer cleaning, oxidation, and metallization were accomplished in a systematic sequence with no delays or storage periods. To monitor accidental contamination introduced during steps other than oxidation, each lot of four processed wafers was divided into two groups of two wafers each. Two control wafers were oxidized in a conventional single-wall,

---

*The metallization pattern was taken from the fourth level of the NBS-3 mask set.[26] Four capacitors of 381-µm diameter are available per cell and each cell is repeated across the wafer at 5.08-mm intervals. Three of the four capacitors have guard rings to control surface current if necessary.

fused-silica oxidation tube provided with a liner;[†] the other two wafers were divided into halves along a diameter[††] and oxidized in the double-wall tube. With the exception of the oxidation step, the lot of four wafers was processed as a unit. The data on the control MOS capacitors were used to gauge the uniformity in the lot processing during the experiment.

The mobile-ion density of the thermal silicon dioxide films was determined from the flat band voltage shift of the MOS capacitors induced by bias-temperature-stress (BTS) testing using cycles of ±10 V at 300°C for 5 min. The resulting electric field applied across the oxide film is about 10^6 V/cm. The capacitance versus voltage (C-V) measurements were made at room temperature using a commercial capacitance bridge operating at 1 MHz with an applied test signal of 15 mV. Although the entire wafer was temperature stressed for each BTS cycle, only specific capacitors (about 8 on each wafer) were bias stressed for a given BTS test. Assuming that the flat-band voltage shift is due entirely to the change in position of the mobile ions with respect to the silicon dioxide-silicon interface, the density of mobile ions, Q_o/q, is given in cm^{-2} by the expression:[27]

$$\frac{Q_o}{q} = \Delta V_{fb} \frac{C_o}{q} = \Delta V_{fb} \frac{\varepsilon\, \varepsilon_o}{qX_o} \quad .$$

where ΔV_{fb} is the change in the flat-band voltage (V) observed as a result of the BTS test, C_o is the oxide film capacitance per unit area (F/cm^2), ε is the relative dielectric constant of the oxide, ε_o is the permittivity of the free space (F/cm), X_o is the oxide film thickness (cm), and q is the electronic charge.

3. Experimental Results

The results reported here were obtained during a time period of more than one year. Figure 2 shows the mobile-ion density in the MOS capacitors prepared in the double-wall tube. The dot on each bar is the average value of the span of data represented by the vertical bar. The variation of the mobile-ion density for a given data point represents the spread of the data taken over the complete lot of processed half wafers. This variation shows nonuniformity of the mobile-ion density with

---

[†] The single-wall oxidation tube used a fused silica liner separated from the oxidation tube by quartz wool. The space between the liner and the oxidation tube was not sealed from the room air. The inner tube was periodically cleaned *in situ* for several hours with 5-percent hydrogen chloride diluted in dry nitrogen.

[††] The diameter of the double-wall oxidation tube was such that only half-wafers (divided along a diameter) could be processed.
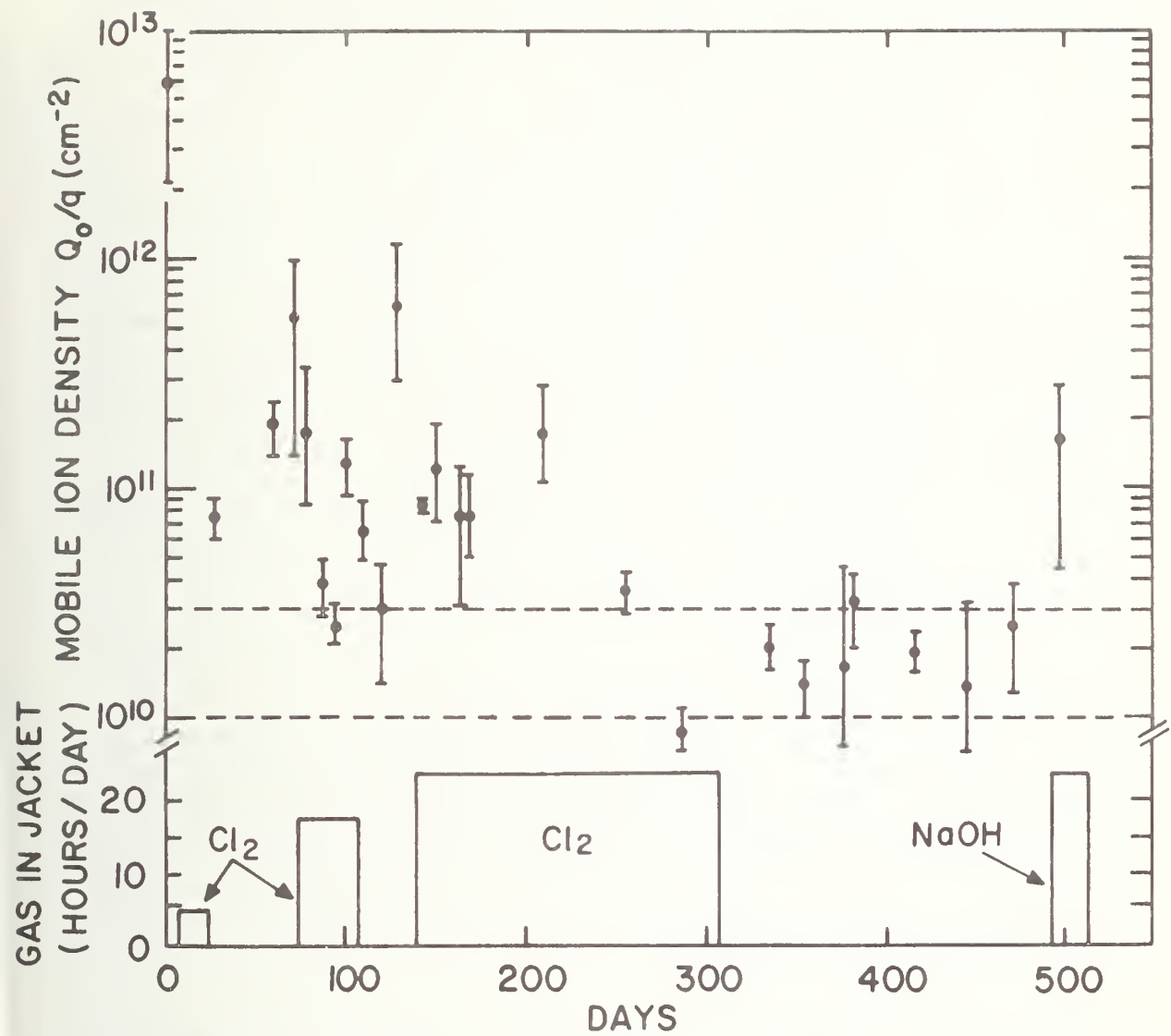
Figure 2. Mobile-ion density in oxide films grown in the double-wall oxidation tube with different atmospheres in the jacket. The dot on each bar is the average value of the span of data corresponding to a given wafer lot represented by the bars. The two dashed lines represent the range of mobile-ion density measured on the control wafers. The bottom part shows periods when chlorine, room air, or sodium hydroxide gas is allowed to fill the jacket.

7

position on the wafer and does not reflect the measurement precision. (The technique is capable of resolving mobile-ion densities in the range of 4×10^9 cm^{-2} for 100-nm thick oxides.) Such variation could possibly be interpreted in terms of localized clustering of the mobile ions.[28] The dashed lines represent the range of mobile-ion density of the control wafers with oxide films prepared in the single-wall oxidation tube. The bottom part shows the periods with chlorine, room air, and sodium hydroxide in the jacket. During the first, second, and third chlorine periods the gas was allowed to flow into the jacket for 5, 18, and 24 hours per day, respectively, while the quartz-wool plug was inserted into the exhaust port of the jacket. This allowed a gradual treatment of the tube with increasing chlorine concentration in the jacket.

After 200 days from the end of the last chlorine cleaning period, external contamination was introduced into the jacket. Nitrogen was passed through a one-percent sodium hydroxide solution at room temperature and the resulting gas was allowed to flow into the jacket for a period of 181 h. Silicon dioxide films were grown during this period with sodium hydroxide in the jacket. The mobile-ion density in the oxide films was measured and an order-of-magnitude increase was observed (see fig. 2). This is due to sodium contamination in the oxidation atmosphere resulting from the passage of sodium through the tube wall.

The initial mobile-ion density in the 10^{12} to 10^{13} cm^{-2} range corresponds to MOS capacitors prepared on wafers which were processed prior to the first chlorine period; the double-wall tube initially had been installed in the furnace with no previous tube clean-up. The data show that the first two chlorine periods were not effective in achieving complete cleaning of the oxidation atmosphere. By the end of the third chlorine period the double-wall tube data are comparable to mobile-ion density data corresponding to control wafers processed in the single-wall oxidation tube. After the third chlorine period, contamination levels in oxides grown in both the double-wall and the single-wall oxidation tubes were similar. This result that was consistently observed for about 200 days is extremely encouraging considering that the tube was initially severely contaminated.

In order to investigate the possibility of chlorine from the jacket diffusing through the tube wall and becoming part of the oxidation ambient and thus passivating the mobile-ion content of the oxide, neutron activation analysis was used to obtain a measure of chlorine in the oxide films prepared in both the double-wall and the single-wall oxidation tubes. Samples of area about 1 cm^2 were packaged in pure polyethylene bags and irradiated in the NBS reactor for periods of 10 and 20 min to thermal neutron fluences of 1.5 to 3×10^{16} cm^{-2}. These results indicate that the chlorine content in oxide films prepared in both the single-wall and the double-wall tubes during chlorine periods is about the same and equal to 10 ppb. Similar results obtained on plain unoxidized silicon substrates indicate higher chlorine content, presumably due to residual chlorine left on the wafers after the cleaning procedure.[25]

8

4. Discussion

The results presented here suggest that the mobile-ion density in oxide films prepared in the double-wall fused-silica oxidation tube is influenced by the atmosphere established in the jacket. The first oxide film was grown immediately after the tube was installed in the furnace. The tube was not cleaned prior to installation and the jacket was open to the room air. The corresponding mobile-ion density resulted in the high 10^{12} cm^{-2} range. During the next 100 days, chlorine was used for two short periods separated by an interval with room air in the jacket. Oxide films grown during these 100 days show a one-order-of-magnitude reduction in the mobile-ion density. After the third chlorine period, room air was allowed into the jacket and several oxides were grown at various times during an interval of about 180 days. These oxides consistently exhibited mobile-ion densities within the range of control oxides prepared in the single-wall tube. This represents a reduction of two orders of magnitude in mobile-ion density with respect to the initial result. By using sodium hydroxide contamination in the jacket, the mobile-ion density was increased again by one order of magnitude. Both the cleaning action of chlorine and the contaminating action of the sodium hydroxide occur through the tube wall. A model describing the interactions in the tube with the jacket atmosphere would be valuable to interpret the present results. More theoretical and experimental work is required to understand the permeability of fused silica at 1000°C to various gases.

Neutron activation analysis results indicate that the chlorine content in oxides grown in the double-wall oxidation tube is only about 10 ppb (about 10^{14} cm^{-3}). These results are consistent with results from ellipsometric determination of the index of refraction of these oxides at wavelength 632.8 nm where no significant departures from the nominal value n = 1.462 are observed. Changes in the index of refraction of Δn = 0.0018 to - 0.0079 have been reported in silicon dioxide films grown in oxygen with the addition of 0.5 to 2 volume percent chlorine at 1000°C.[29] Experimental evidence shows that thermal silicon dioxide films grown at 1100°C in one-percent hydrogen chloride in oxygen on (111) phosphorus-doped 10 $\Omega \cdot cm$ silicon wafers contain large amounts of chlorine. The residual chlorine profile measured by the Rutherford backscattering technique using a 2 MeV-^{4}He beam indicates a chlorine content in these oxides higher than 10^{20} cm^{-3}.[30]

Oxide films grown in the double-wall oxidation tube may also be of interest for fabricating radiation hardened devices. Although it has been established that there is little correlation between mobile-ion contamination in silicon dioxide films and radiation sensitivity of MOS devices, it has been recognized that the use of hydrogen chloride during oxidation to reduce the mobile-ion content in these films increases the device radiation sensitivity.[31] Although the radiation sensitivity of the oxides produced in the double-wall tube has not been investigated, the technique provides an alternative to present radiation-hard oxide preparation methods requiring extensive hydrogen chloride tube cleaning

periods prior to the oxide growth.[31] The double-wall oxidation tube with the chlorine barrier requires no specific cleaning of the oxidation chamber. Hence, in principle, oxidation can occur on a continuous basis with no interruptions for routine clean-ups as required by the conventional hydrogen chloride oxidation chamber cleaning. However, additional experimental work is required to completely characterize these oxides.

Acknowledgment

References

1. Hickmott, T. W., Thermally Stimulated Conductivity of Sodium in Thermal SiO_2, *J. Appl. Phys.* <u>46</u>, 2583-2598 (1975).

2. Deal, B. E., The Current Understanding of Charges in the Thermally Oxidized Silicon Structure, *J. Electrochem. Soc.* <u>121</u>, 198C-205C (1974) and Charge Effects and Other Properties of the SiO_2-Si Interface: The Current Understanding, *Semiconductor Silicon 1977*, H. R. Huff and E. Sirtl, Eds., pp. 276-296. Proceedings of the Third International Symposium on Silicon Materials Science and Technology, The Electrochemical Soc., Inc. (1977).

3. Derbenwick, G. F., Mobile Ions in SiO_2: Potassium, *J. Appl. Phys.* <u>48</u>, 1127-1130 (1977).

4. Yurash, B., and Deal, B. E., A Method of Determining Sodium Content of Semiconductor Processing Materials, *J. Electrochem. Soc.* <u>115</u>, 1191-1196 (1968).

5. Knolle, W. R., and Retajczyk, T. F., Jr., Monitoring Sodium Contamination in Silicon Devices and Processing Materials by Flame Emission Spectrometry, *J. Electrochem. Soc.* <u>120</u>, 1106-1111 (1973).

6. Kerr, D. R., Logan, J. S., Burkhardt, P. J., and Pliskin, W. A., Stabilization of SiO_2 Passivation Layers with P_2O_5, *IBM J. Res. Develop.* <u>8</u>, 376-384 (1964).

7. Eldridge, J. M., Sodium Drift Through Phosphosilicate Glass-SiO_2 Films, *J. Electrochem. Soc.* <u>118</u>, 986-991 (1971), Balk, P., and Eldridge, J. M., Phosphosilicate Glass Stabilization of FET Devices, *Proc. IEEE* <u>57</u>, 1558-1563 (1969).

8. Kriegler, R. J., Cheng, Y. C., and Colton, D. R., The Effect of HCl and Cl_2 on the Thermal Oxidation of Silicon, *J. Electrochem. Soc.* <u>119</u>, 388-392 (1972).

9. Kriegler, R. J., Neutralization of Na^+ Ions in "HCl-Grown" SiO_2, *Appl. Phys. Lett.* 20, 499-451 (1972).

10. Kriegler, R. J., The Role of HCl in the Passivation of MOS Structures, *Thin Solid Films* 13, 11-14 (1972).

11. Mayo, S., Keller, R. A., Travis, J. C., and Green, R. B., Detection of Sodium Trace Contamination in Furnace Atmospheres at 1000°C, *J. Appl. Phys.* 47, 4012-4106 (1976).

12. Hetherington, G., Stephenson, G. W., and Winterburn, J. A., Vitreous Silica in Electronics, *Electronic Engineering* 41, No. 495, 5256, and No. 496, 4447 (1969).

13. Owen, A. E., and Douglas, R. W., The Electrical Properties of Vitreous Silica, *J. Soc. Glass Technology* 43, 159T-178T (1969).

14. Dietze, W., Hunt, L. P., and Sawyer, D. H., The Preparation of CVD-Silicon Tubes and Boats for Semiconductor Device Technology, *J. Electrochem. Soc.* 121, 1112-1115 (1974).

15. Fewer, D. R., and Gill, W. L., Investigation of Reliability Testing and Prediction Techniques for Integrated Circuits, Technical Report No. RADC-TR-66-345, pp. 33-46 (1966). Also available as NTIS Document AD-489-969.

16. Vidale, G. L., Measurement of the Absorption of Resonance Lines III, Vaporization of Sodium from Sodium Silicate Glasses, General Electric Co., Technical Information Series, R60SD390 (1960).

17. Mayo, S., and Evans, W. H., Development of Sodium Contamination in Semiconductor Oxidation Atmospheres at 1000°C, *J. Electrochem. Soc.* 124, 780-785 (1977).

18. Mayo, S., and Evans, W. H., Thermodynamic Considerations in the Use of Polysilicon Oxidation Tubes for Clean SiO_2-Film Preparation, *J. Electrochem. Soc.* 125, 106-110 (1978).

19. Wolf, H. F., *Silicon Semiconductor Data*, pp. 526-527 (Pergamon Press, Oxford, 1969).

20. Matheson Gas Products, Oxygen Data Sheet.

21. Revesz, A. G., Noncrystalline Silicon Dioxide Film on Silicon: A Review, *J. Noncrystalline Solids* 11, 309-330 (1970).

22. Irene, E. A., The Effects of Trace Amounts of Water on the Thermal Oxidation of Silicon in Oxygen, *J. Electrochem. Soc.* 121, 1613-1616 (1974).

23. Irene, E. A., and van der Meulen, Y. J., Silicon Oxidation Studies: Analysis of SiO_2 Film Growth Data, *J. Electrochem. Soc.* <u>123</u>, 1380-1384 (1976).

24. Irene, E. A., and Ghez, R., Silicon Oxidation Studies: The Role of H_2O, *Semiconductor Silicon 1977*, H. R. Huff and E. Sirtl, Eds., pp. 313-323 (The Electrochemical Society, Princeton, 1977).

25. Kern, W., and Puotinen, D. A., Cleaning Solutions Based on Hydrogen Peroxide for Use in Silicon Semiconductor Technology, *RCA Review* <u>31</u>, 187-206 (1970).

26. Buehler, M. G., Microelectronic Test Pattern NBS-3 for Evaluating the Resistivity Dopant Density Relationship of Silicon, NBS Special Publication 400-22 (June 1976).

27. Grove, A. S., *Physics of Semiconductor Devices*, p. 339 (J. Wiley and Sons, Inc., New York, 1967).

28. DiStefano, T. H., Dielectric Breakdown Induced by Sodium in MOS Structures, *J. Appl. Phys.* <u>44</u>, 527-528 (1973). DiStefano, T. H., and Viggiano, J. M., Interface Imaging by Scanning Internal Photo-emission, *IBM J. Res. Develop.* <u>18</u>, 94-99 (1974).

29. van der Meulen, Y. J., Osburn, C. M., and Ziegler, J. F., Proper-ties of SiO_2 Grown in the Presence of HCl on Cl_2, *J. Electrochem. Soc.* <u>122</u>, 284-290 (1975).

30. Meek, R. L., Residual Chlorine in O_2: HCl Grown SiO_2, *J. Electro-chem. Soc.* <u>120</u>, 308-310 (1973).

31. Gregory, B. L., Process Controls for Radiation-Hardened Aluminum Gate Bulk Silicon CMOS, *IEEE Trans. Nucl. Sci.* <u>NS-22</u>, 2295-2302 (1975).

Detection of sodium trace contamination in furnace atmospheres at 1000°C*

Santos Mayo

Electronic Technology Division, Institute for Applied Technology, National Bureau of Standards, Washington, D.C. 20234

Richard A. Keller

Physical Chemistry Division, Institute for Materials Research, National Bureau of Standards, Washington, D.C. 20234

John C. Travis and Robert B. Green

Analytical Chemistry Division, Institute for Materials Research, National Bureau of Standards, Washington, D.C. 20234
(Received 12 May 1976)

Free sodium atoms were detected by resonance fluorescence in an open contaminated quartz tube heated to 1000°C. The quartz tube and furnace were similar to those used in semiconductor device processing. Fluorescence was excited by a cw dye laser tuned to the sodium D_1 or D_2 transition and directed along the axis of the furnace. Fluorescence from the sodium D_2 line emitted in the axial direction was collected by a telescopic system and focused onto a photomultiplier tube. The estimated minimum detectable sodium density in the furnace is 5×10^5 atoms/cm^3. No free sodium was detectable in a processing tube that had not been intentionally contaminated.

I. INTRODUCTION

Sodium contamination in microelectronic devices has been correlated with erratic electrical behavior of these devices.[1] The electrical properties of silicon dioxide films in metal-oxide-semiconductor (MOS) devices have been the subject of many investigations in which sodium was shown to be one of the principal causes of instabilities.[2] Among other sources of sodium contamination such as those due to materials associated with the processing of semiconductor devices,[3] the oxidation furnace atmosphere itself was suggested as a prominent one because of the high diffusion coefficient of sodium in silicon and silicon dioxide at temperatures used for oxidation.[4] It has been postulated that sodium is transferred from the furnace material to the silicon wafer through the furnace atmosphere as free sodium atoms. Contamination control during device processing has been highly recommended to produce radiation hardened stable MOS devices. The mechanisms by which alkali contamination affects hardness are not well established[5] although ion microprobe studies of MOS devices show a correlation of sodium content in the oxide with radiation sensitivity.[6] The purpose of this work is to develop a measurement technique for measuring sodium impurities in furnace atmospheres used in the growth of MOS oxides and in their subsequent annealing.

It is difficult to detect free sodium atoms at atmospheric concentration levels concomitant with the observed device contamination. Atomic absorption techniques are limited to concentration ranges above 10^8 atoms/cm^3 by the difficulty of measuring small changes in transmitted light.[7,8]

Sodium concentrations as small as 100 atoms/cm^3 were recently detected in an evacuated tube at -28°C by a resonance fluorescence technique.[9-11] This paper reports on an extension of this method to an open quartz tube at 1000°C. Problems associated with Doppler and collisional cross-section reduction, reaction of the sodium with oxygen and water, quenching of the emission by molecular collisions, and scattering from furnace gases, thermal gradients, suspended dust particles, and geometrical restrictions related to the structure of the furnace result in a poorer detection limit.

II. EXPERIMENTAL METHOD

A diagram of the apparatus used for the detection of resonance fluorescence from sodium vapor is shown in
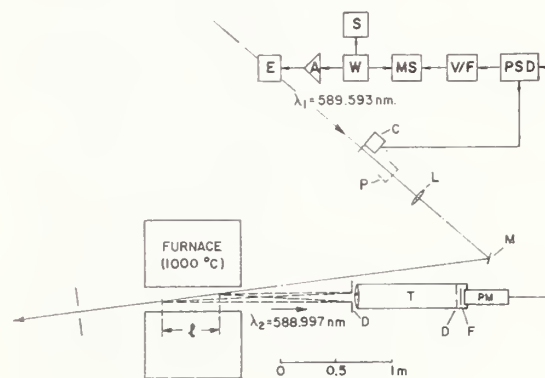

FIG. 1. Experimental arrangement for sodium detection in a semiconductor processing furnace. E, 0.5-mm etalon mounted on torsion motor; A, power amplifier; W, sinusoidal wave generator (0.5 Hz); S, sweep counter; MS, multiscaler; V/F, voltage to frequency converter; PSD, phase sensitive detector; C, chopper (2 kHz); P, power meter; L, lens; M, mirror; T, telescope; D, diaphragm; F, interference filter (1.25-nm FWHM, 588.5 nm); PM, photomultiplier tube; l, length of observation region.
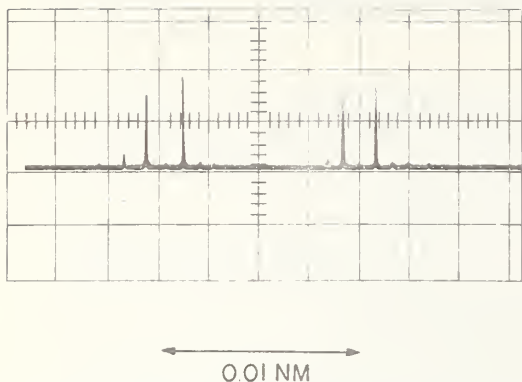
13

0.01 NM

FIG. 2. Typical laser beam mode structure. The repetition of the pattern is due to the two spectral ranges covered by the spectrum analyzer.

Fig. 1. Amplitude-modulated radiation from a tunable dye laser passes down the furnace slightly off axis (2°) and through a hole in the laboratory wall. The fluorescence emission traveling out of the tube in the direction opposite to the laser beam is collected by a telescopic system, passed through an interference filter (centered on the D_2 line), and focused onto a photomultiplier tube. The ac signal corresponding to the fluorescence is synchronously detected, digitized, and recorded on a multichannel analyzer as a function of the wavelength of the excitation laser.

The excitation source was a commerical cw dye laser which was longitudinally pumped with powers up to 5 W by an all-line argon-ion cw laser. An intracavity birefringent filter was used to coarse tune the dye laser with a resultant bandwidth of 0.03 nm. Insertion of a 0.5-mm etalon into the cavity further narrowed the output to 0.003 nm. The mode structure of the dye laser was monitored by observing a small fraction of the beam with an interferometric spectrum analyzer (8-GHz free spectral range). A typical mode structure is shown in Fig. 2. These laser modes fall within the broadened absorption line of sodium (~ 0.01 nm). The laser emission wavelength could be repetitively and reproducibly scanned over the absorption line by rotating the etalon through an angle of about 1° with an oscillatory torsion motor driven by a low-frequency (0.5 Hz) low-amplitude sinusoidal wave. The laser was tuned to center the sodium D_1 resonance on the approximately linear portion of the sinusoidal wavelength scan. The signal-to-noise ratio was increased by repetitive scanning of the laser wavelength and summing the data from approximately 100 sweeps in the multichannel analyzer. The wavelength scale was calibrated by passing a portion of the output of the laser through the spectrum analyzer.

A major limitation to the minimum observable sodium signal was scattered laser light. Extreme care was necessary in the placement of optical components, apertures, and the dumping of the laser beam to minimize back reflection. Contributions from scattered light were further reduced by excitation of the D_1 line (589.6 nm) and observation of the D_2 emission (589.0 nm). At at-

mospheric pressure, collisions with molecular nitrogen and oxygen in the furnace completely equilibrate the population of these two levels according to their statistical weights. [12,13]

The calibration necessary to relate the density of sodium atoms to the observed fluorescence signal was done by two methods. The first method involved a comparison of the fluorescence intensity from the sodium with the fluorescence intensity from a dilute solution of rhodamine 6G placed in a glass cell in the cooled furnace. The dimensions of the glass cell were the same as those of the quartz tube. The second method was based upon a calculation of the geometric factors involved in the detection optics and a measurement of the ratio of the intensity of the fluorescence emission to the excitation intensity. The methods yielded results that agreed within a factor of 3.

Sodium fluorescence signals were not observable in clean quartz tubes. Nonquantitative sodium contamination was intentionally introduced by aspirating dilute sodium chloride solutions into the hot tube for short periods of time and then waiting for several hours until a relatively constant level of contamination was observed.

III. FLUORESCENCE SIGNAL RESULTS

The fluorescence signal from sodium vapor inside of the quartz tube is shown in Fig. 3. These data are the accumulation of 100 2-sec sweeps. The average excitation power was 70 mW. The observed linewidth of the excitation spectrum (7.5 GHz or ~ 0.01 nm) agrees well with the calculated linewidth taking into account Doppler (2.7 GHz) and pressure (6.2 GHz) broadenings under the conditions of the experiment. This good agreement is indicative of the frequency stability of the laser system. Background blackbody emission from the furnace was discriminated against by the sodium interference filter and synchronous detection. The nonzero signal observed off resonance is caused by scattered laser light. The scattered light signal is reduced approximately an order of magnitude when the D_1 tran-
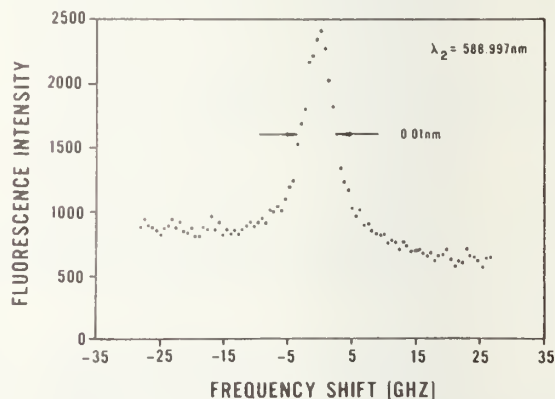

FIG. 3. Sodium fluorescence signal detected in contaminated furnace atmosphere pressure, 1000 °C. This signal corresponds to 2.5×10^7 sodium atoms/cm^3.

14

$I_R(589.0)/I_{Na}(589.0)$	0.19 [a]	$I_0(589.6)$	70 mW [a]
$\sigma_R(571.8)$	2.4×10^{-18} cm^2 [a]	Q_R	0.85 (Ref. 14)
$\sigma_{Na}(589.6)$	7.9×10^{-13} cm^2 [b]	Q_{Na}	$0.01 - 0.04$ (Refs. 15 and 16)
N_R	3.5×10^{13}/cm^3 [a]	A_R	6.1×10^{-3} [b]
$I_0(571.8)$	9.0 mW [a]	A_{Na}	0.31 [b]

[a] Experimentally determined. [b] Calculated.

sition is excited and the D_2 emission observed, in agreement with the transmission characteristics of the interference filter. Any reduction in the absolute magnitude of the scattered light results in a reduction in the associated shot noise and in noise resulting from fluctuations in the scattering medium. After careful alignment of the optical system, a major contribution to the scattered light was reflections from suspended dust particles in the tube. This contribution could be reduced by flushing the tube with clean nitrogen. A statistical analysis of the data in Fig. 3 shows that the ratio of the fluorescence signal at the peak to the noise in the scattered light is > 50. The long-term precision is better than 10%.

IV. CALIBRATION 1

The quartz tube was replaced by a room-temperature cell containing a dilute solution of rhodamine 6G dissolved in ethyl alcohol. Absorption cross sections and fluorescence quantum yields for this material are well known.[14] For the measurement of the fluorescence intensity at the wavelength of the sodium D_2 line, it was expedient to irradiate at a shorter wavelength to provide a reasonable cross section and to reduce scattered light from the windows of the cell and dust particles in the liquid. A convenient wavelength was found to be around 570 nm. The laser beam was deflected by the solution and windows on the cell, requiring a slight realignment of the optics to maximize the fluorescence signal and minimize the scattered light.

The calibration process can be understood by considering the following equations:

$$I_R(589.0) = \sigma_R(571.8)N_R l I_0(571.8)Q_R A_R G, \qquad (1)$$

$$I_{Na}(589.0) = \sigma_{Na}(589.6)N_{Na} l I_0(589.6)Q_{Na} A_{Na} G . \qquad (2)$$

I_R and I_{Na} are the measured fluorescence intensities from rhodamine and sodium, the σ's are the absorption cross sections at the indicated wavelengths, the N's are atomic or molecular densities, l is the length from which fluorescence is being detected, the Q's are fluorescence quantum yields, the A's are the spectral fraction of the emitted light passed by the interference filter, and G is a geometric collection factor assumed similar for both samples. Taking the ratio of Eq. (1) and Eq. (2) and solving for N_{Na} gives Eq. (3),

$$N_{Na} = N_R \frac{I_{Na}(589.0)}{I_R(589.0)} \frac{\sigma_R(571.8)}{\sigma_{Na}(589.6)} \frac{I_0(571.8)}{I_0(589.6)} \frac{Q_R}{Q_{Na}} \frac{A_R}{A_{Na}} . \qquad (3)$$

All quantities in Eq. (3) are known or can be measured. A_R is found by folding the transmission curve of the

interference filter $[T(\lambda)]$ into the spectral emission curve of the dye $[F(\lambda)]$.

$$A_R = \int T(\lambda)F(\lambda)\,d\lambda / \int F(\lambda)\,d\lambda. \qquad (4)$$

A_{Na} is calculated by assuming equal population among the substates of D_1 and D_2 levels and including the effects of the interference filter,

$$A_{Na} = \frac{2}{(4+2)} T(589.6) + \frac{4}{(4+2)} T(589.0).$$

The statistical weights of the D_1 and D_2 levels are 2 and 4 respectively. σ_{Na} can be calculated from the oscillator strength and the calculated linewidth contributions.[13] The quantities for Eq. (3) are given in Table I.[15,16]

V. CALIBRATION 2

Equation (2) relates the observed fluorescence intensity to the density of sodium atoms. Rearrangement of this equation for the case where both excitation and observation are at 589.0 nm gives

$$N_{Na} = \frac{I_{Na}(589.0)}{I_0(589.0)} [\sigma_{Na}(589.0) l Q_{Na} A_{Na} G]^{-1}. \qquad (6)$$

All quantities to the right of the equality sign are known or can be measured. The values of σ, l, Q, and A are listed in Tables I and II. The intensities of the sodium fluorescence and laser excitation were measured by comparison with an electrically calibrated pyroelectric detector.[17] Neutral-density filters were used with PIN diodes to change intensities in known ratio, into the range of linearity for these devices. The geometric collection factor was evaluated by consideration of the optical design shown in Fig. 1.

The results of both calibrations are listed in Table III. The data for calibration 2 were preliminary and are recorded here only as an independent check on later results.

VI. OXIDE IMPURITY RESULTS

A clean (the quartz tube was rinsed in hydrofluoric and nitric acid solutions and washed in deionized water)

TABLE II. Additional constants for calibration with calculated geometric factors.

$\sigma_{Na}(589.0)$	1.5×10^{-12} cm^2 [a]	G	5.5×10^{-4} [a]
$I_{Na}(589.0)$	360 pW [b]	l	60 cm [b]
$I_0(589.0)$	140 mW [b]		

[a] Calculated. [b] Experimentally determined.

Calibration	Na density (atoms/cm^3)	S/N	Minimum detectable quantity [b] (atoms/cm^3)
1 (rhodamine)	$3-12 \times 10^7$	56	$5-20 \times 10^5$
2 (geometric)	$4-16 \times 10^6$	22	$2-8 \times 10^5$

[a] Range reflects uncertainty in Q_{Na}.
[b] Signal to noise equal to two.

quartz furnace tube with end caps was used to grow oxide films on silicon wafers. After the oxide film was prepared, the end caps were removed (water from ambient humidity may have diffused into the tube during the measurement; see Sec. VII) and it was found that no sodium fluorescence was observable within the detection limits reported in Table III. The oxide films grown on silicon in this clean tube showed an order of magnitude higher sodium contamination level than is normally present on similar films prepared in production-type semiconductor processing oxidation tubes operated in a controlled environment. These results were obtained by capacitance-vs-voltage measurements performed on MOS capacitors after application of simultaneous electric bias and temperature stress cycles. Electric fields of about 10^6 V/cm were established across the oxide film by use of positive or negative 10-V gate polarization while the device temperature is maintained at 300 °C for 10 min (MOS-CV-BT stress technique).[18]

Similar oxide layers were grown on silicon in a sodium-contaminated oxidation tube where sodium fluorescence from approximately 10^7 atoms/cm^3 was measureable. MOS capacitors built on this oxide exhibited two orders of magnitude more sodium content than similar control capacitors prepared in a standard processing facility as measured by the MOS-CV-BT stress technique.

VII. DISCUSSION

It is important to note that the technique described above is a measurement of free sodium atoms only. Sodium present in compounds (e.g., Na_2O and $NaOH$) would not be detected. These results are important for understanding the apparent discrepancy between the oxide impurity measurements and the resonance fluorescence results. It is a difficult thermodynamic problem to estimate the concentration of oxides and the hydroxide from a knowledge of the free sodium concentration because the concentrations of other species (e.g., H_2 and OH) are uncertain by many orders of magnitude. It should be possible to measure the hydroxyl radical concentration in the furnace by a similar resonance fluorescence technique.[19] Knowledge of both the free sodium and the hydroxyl radical concentration could be used to determine the sodium hydroxide concentration.

In a production semiconductor processing furnace, where the oxidation atmosphere is completely enclosed in the quartz tube and carefully controlled dry oxygen is used, a more favorable ratio of free sodium to total

sodium might be expected. Such conditions would improve the atomic measurement except for additional sources of light scattering at the capped tube ends. However, these sources of interference could be practically eliminated by an alternative geometry discussed below.

There are several improvements which should decrease the detection limits reported above. The first of these involves frequency modulation of the excitation beam and synchronous detection of the fluorescence to reduce contributions from frequency-independent scattering. Frequency modulation of the cw dye laser is relatively straightforward.

Scattered light could be significantly reduced by using a monochromator in place of the interference filter to completely isolate the D_1 excitation from the D_2 emission. The insertion of the monochromator may reduce the total number of photons reaching the photomultiplier tube to the extent that photon counting might be necessary.

A reduction of scattered light and an increase in light gathering power could be accomplished by mounting the detecting optics in ports distributed down the tube and viewing the fluorescence at right angles to the excitation. This has two additional advantages: (1) information on the spatial distribution of the contamination would now be available by viewing through different ports; (2) windows on the quartz tube would not interfere with the measurement because laser scattering from them would be far from the field of view subtended by the detector.

ACKNOWLEDGMENTS

*This research was conducted under the joint auspices of the Semiconductor Technology Program and the Laser Chemistry Program of the National Bureau of Standards. Partial support was provided by the Defense Nuclear Agency.
[1] R. J. Kriegler, 12th Annual Proceedings Reliability Physics 1974 (IEEE, New York, 1974), p. 250.
[2] T. W. Hickmott, J. Appl. Phys. 46, 2583 (1975).
[3] B. Yurash and B. E. Deal, J. Electrochem. Soc. 115, 1191 (1968).
[4] D. R. Fewer and W. L. Gell, Texas Instruments Inc., Technical Report No. RADC-TR-66-345, 1966 (unpublished).
[5] B. L. Gregory, IEEE Trans. Nucl. Sci. NS-22, 2295 (1975).
[6] H. Hughes, R. D. Baxter, and B. Phillips, IEEE Trans. Nucl. Sci. NS-19, 256 (1972).
[7] T. E. Burgess and H. M. Donega, J. Electrochem. Soc. 116, 1313 (1969).
[8] N. Ioli, F. Strumia, and A. Moretti, J. Opt. Soc. Am. 61, 1251 (1971).

16

[9]D. A. Jennings and R. A. Keller, J. Am. Chem. Soc. **94**, 9249 (1972).

[10]W. M. Fairbank, Jr., T. W. Hänsch, and A. L. Schawlow, J. Opt. Soc. Am. **65**, 199 (1975).

[11]F. C. M. Coolen and H. L. Hagedoorn, J. Opt. Soc. Am. **65**, 952 (1975).

[12]M. Stupavsky and L. Krause, Can. J. Phys. **46**, 2127 (1968).

[13]A. C. G. Mitchell and M. W. Zemansky, *Resonance Radiation and Excited Atoms* (Cambridge U. P., Cambridge, England, 1971), p. 100.

[14]J. P. Webb, W. C. McColgin, O. G. Peterson, D. L. Stockman, and J. H. Eberly, J. Chem. Phys. **53**, 4227 (1970).

[15]D. R. Jenkins, Proc. R. Soc. London A **293**, 493 (1966).

[16]H. P. Hooymayers and C. Th. J. Alkemade, J. Quant. Spectrosc. Radiat. Transfer 6, 847 (1966).

[17]J. Geist, B. Steiner, R. Schaefer, E. Zalewski, and A. Corrons, Appl. Phys. Lett. **26**, 309 (1975).

[18]R. Y. Koyama and M. G. Buehler, *Semiconductor Measurement Technology*, edited by W. M. Bullis, NBS Special Publication No. 400-4 (U. S. GPO, Washington, D. C., 1974), pp. 37—39.

[19]C. C. Wang and L. I. Davis, Jr., Phys. Rev. Lett. **32**, 349 (1974).

4016   J. Appl. Phys., Vol. 47, No. 9, September 1976

Mayo *et al.*   4016

17

Development of Sodium Contamination in Semiconductor Oxidation Atmospheres at 1000°C

Santos Mayo

Electronic Technology Division, Institute for Applied Technology,
National Bureau of Standards, Washington, D.C. 20234

and William H. Evans

National Bureau of Standards, Physical Chemistry Division,
Institute for Materials Research, Washington, D.C. 20234

19

Development of Sodium Contamination in Semiconductor Oxidation Atmospheres at 1000°C

Santos Mayo

Electronic Technology Division, Institute for Applied Technology,
National Bureau of Standards, Washington, D.C. 20234

and William H. Evans

National Bureau of Standards, Physical Chemistry Division,
Institute for Materials Research, Washington, D.C. 20234

ABSTRACT

The thermodynamic equilibria established in fused silica oxidation tubes operated at 1000°C are analyzed. Transparent fused silica tubes used for thermal oxidation of silicon contain about 10 ppm sodium impurity. At oxidation temperatures sodium diffuses in fused silica, evaporates into the oxidation ambient, and reacts with residual water contaminating the oxidation atmosphere. During the oxidation cycle enough sodium is incorporated into the growing oxide film to be detected later by capacitance measurements in metal oxide semiconductor (MOS) structures. Reactions taking place during currently used *in situ* furnace cleaning procedures are analyzed. Calculations indicate that the amount of sodium removed from the fused silica tube wall through chlorine or hydrogen chloride cleaning is substantial. The reaction rate is regulated by diffusion of sodium in the fused silica. The use of iodine and hydrogen iodide as cleaning agents is discussed.

Oxidation of silicon has been the subject of many investigations aimed at understanding metal oxide semiconductor (MOS) device instabilities caused by the action of mobile ion impurities localized in the oxide film (1). Test vehicles in the form of simple MOS capacitors built on silicon dioxide films 50-100 nm thick are frequently used to study ionic contamination in thermal silicon dioxide. The mobile ion density in the oxide film can be calculated from capacitance measurements after thermal cycles have been applied to the device (2).

Several contamination sources may contribute impurities to the oxide film. Due to their high natural abundance, alkali species are the most common impurities likely to contaminate silicon dioxide. Sodium, potassium, and lithium may cause ionic-type instabilities in the oxide. Sources of alkali contamination can be classified according to their origin as: (i) bulk and surface impurities already contained in the silicon wafer before oxidation, (ii) impurities introduced into the oxide film during silicon high temperature oxidation and annealing, and (iii) impurities introduced after oxidation through metallization (3).

Considerable research has been done to determine the presence of impurities in microelectronic process materials. Analytical techniques such as flame emission, atomic absorption, resonance fluorescence, neutron activation, and others have been used for trace contamination detection (4-6). Metallization of microelectronic devices has also received a great deal of attention regarding the introduction of ionic contamination in the oxide film from both the evaporation process used and contamination in the metal (7). These results show that impurities may be introduced through several processing steps and play a significant role in determining the electrical properties of the device.

During oxidation of silicon, sodium impurity contained in fused silica oxidation tubes evaporates from the tube wall into the oxidation ambient. In typical oxidation facilities, furnaces employing fused silica tubes are operated at about 1000°C (or 1300°K for

the purpose of this paper). The oxidation atmosphere generally consists of pure dry oxygen flowing along the tube with laminar flow at about 4 cm³/sec (equivalent to 0.5 std ft³/hr). Transparent commercial fused silica tubes currently used for this purpose generally have an average sodium content of 10 ppm (8-9). Sodium in the tube bulk diffuses easily [diffusion coefficient in SiO_2: 2×10^{-6} cm²/sec (10)] to the tube wall surface. This in turn causes the appearance of contamination in silicon dioxide films grown in the oxidation tube (11).

The purpose of this work is to study the oxidation atmosphere used to grow thermal silicon dioxide films as a source of sodium contamination introduced into the film during the growing cycle. The thermodynamic equilibria established in fused silica oxidation tube atmospheres at 1300°K were considered.

Reactions Occurring in Fused Silica Oxidation Tubes

The thermodynamics of sodium vaporization from sodium silicate-silica glasses has been previously studied in the temperature range of 1200°-2000°K where the equilibrium constant of the reaction $Na_2O \cdot SiO_2$ (in SiO_2) → $2Na(g) + \frac{1}{2} O_2(g) + SiO_2$ (c or glass) has been measured (12). Values of $K = p^2(Na) \cdot p^{1/2}(O_2) [a(SiO_2)/a(Na_2O \cdot SiO_2)]$ were reported for molar ratios of SiO_2 to Na_2O varying from 1.69:1 to 3.88:1, where the a's (activities) were expressed in terms of mole fractions. The results indicated Raoult law behavior was approximated in the higher ratio solutions. On this basis, extrapolation to larger ratios, i.e., 10^5 (about 10 ppm sodium in the silica) leads to the value $K = 2.5 \times 10^{-19}$ at $T = 1300°K$. Using this value and thermodynamic data from Table VII we obtain $\Delta H°_{f298}(Na_2O \cdot SiO_2[10^{-5}$ mole fraction in SiO_2 gls]) = -376.8 kcal/mole. This value is in reasonably good agreement with the corresponding JANAF (13) value for $Na_2O \cdot SiO_2(gls)$ of 373.2 kcal/mole. The difference between these values can be considered a measure of the solution effects, such as formation of $Na_2O \cdot x SiO_2$ species, and the difference between the properties of the simple compound as a glass and the same species in solution. For this reason the use

Table 1. Equilibrium atmosphere in fused silica dry oxidation tube at 1300°K. Sodium content in fused silica bulk is 10 ppm, oxygen at 1 atm.

	Reaction	K	p(atm)	N(cm^{-3})
[1]	$\frac{1}{2} O_2(g) \rightarrow O(g)$	1.76×10^{-7}	$p(O) = 1.76 \times 10^{-7}$	
[2]	$Na_2O \cdot SiO_2$ (in SiO_2) $\rightarrow Na_2O(g) + SiO_2(c)$	7.9×10^{-20}	$p(Na_2O) = 7.9 \times 10^{-25}$	
[3]	$Na_2O \cdot SiO_2$ (in SiO_2) $\rightarrow 2Na(g) + \frac{1}{2} O_2(g) + SiO_2(c)$	2.5×10^{-10}	$p(Na) = 1.6 \times 10^{-12}$	9×10^{6}
[4]	$Na_2O \cdot SiO_2$ (in SiO_2) $\rightarrow Na(g) + NaO(g) + SiO_2(c)$	9.1×10^{-20}		
[5]	$Na_2O(g) + \frac{1}{2} O_2(g) \rightarrow 2NaO(g)$	0.42	$p(NaO) = 5.7 \times 10^{-15}$	3.2×10^{6}
[6]	$Na_2O \cdot SiO_2$ (in SiO_2) $+ \frac{1}{2} O_2(g) \rightarrow 2NaO(g) + SiO_2(c)$	3.3×10^{-29}		

Total sodium density: 1.2×10^{7}

of the former value (−376.8 kcal/mole) derived from measurements (12) was preferred, assuming that any systematic errors in the calculations would be partially compensated.

A number of reactions take place in fused silica oxidation tubes operated at 1300°K. Table 1 shows the equilibrium[1] atmosphere resulting from 1 atm dry oxygen reacting with the tube wall. The partial pressure corresponding to atomic oxygen resulting from equilibrium dissociation of the oxygen molecule is shown through reaction [1][2] as $p(O) = 1.76 \times 10^{-7}$ atm indicating that reactions with atomic oxygen are not significant. The evaporation reactions [2], [3], and [4] show that sodium in the oxidation atmosphere is present as both atomic (Na) and molecular (Na_2O, NaO) species. Reaction [5] shows the conversion of Na_2O into NaO through interaction with oxygen. These results indicate that in a dry oxidation atmosphere atomic sodium is about three times more abundant than molecular sodium compounds. The total number of sodium atoms in the equilibrium oxidation atmosphere is 1.2×10^7 cm^{-3} (both atomic and molecular species included).

Table II shows the equilibrium atmosphere resulting in fused silica oxidation tubes at 1300°K when water is added.[3] The reaction system [7] shows that water is more stable than OH by factors ranging from 20 to more than 100 times as humidity in the oxidation ambient increases. For increasing water content the most significant changes are seen in $p(Na_2(OH)_2)$ and p(NaOH) as resulting from reactions [8] through [11]. The sodium number density for 1 ppm water impurity goes to 3.3×10^8 cm^{-3} or a factor 27 higher than the dry oxidation condition. If 30 ppm water is present in the oxidation ambient the sodium number density at equilibrium raises to 1.7×10^9 cm^{-3} or a factor 142 higher than the dry oxidation condition. Table III and Fig. 1 summarize these results.[4]

The above calculations show that sodium contamination developed in oxidation atmospheres could be explained in terms of contamination in the bulk fused silica even if the furnace tube wall surface were perfectly clean. To reduce sodium density in oxidation atmospheres, it is necessary that the bulk tube material itself be sodium free. Two different approaches have been tried: (*i*) use of a sodium-free tube wall,

---

[1] All calculated values presented in this work refer to equilibrium conditions and represent limiting values for the actual systems because of kinetic and diffusion factors.
[2] Data used to calculate reaction equilibrium constants are listed in Table VII. The actual calculation scheme is illustrated in the Appendix.
[3] Experimental evidence shows that in a typical "dry" oxidation atmosphere the water content is in the 20-30 ppm range (14). Moreover at oxidation temperatures in the range 900°-1300°C it was reported that water and/or hydrogen from the external ambient can diffuse through the silica tube wall into the oxidation chamber (15).
[4] Because of errors and approximations involved in thermodynamic data used to evaluate the equilibrium results, an absolute error of ±50% could be expected in these calculations. The relative error is much smaller. Resonance fluorescence measurements showed that in open fused silica oxidation tubes no free sodium was detected (16). This experimental result can be understood in terms of calculations shown in Fig. 1. For sufficiently high water content in the oxidation atmosphere the amount of free sodium detectable through resonance fluorescence technique will be substantially reduced due to sodium reactivity with excess water. Thus, free sodium is converted into compound sodium and consequently becomes not detectable by the above-mentioned technique.

---

or (*ii*) use of sodium-leaching agents to deplete a region just under the inner wall surface prior to oxidations. The first approach is based on the well-known fact that polycrystalline silicon tubes can be produced with 1000 times less sodium content than found in silica tubes (17). Empirical results indicate that oxide films grown on silicon using recently installed silicon oxidation tubes produce cleaner films (lower sodium content) than similar oxides prepared in fused silica tubes.

Polycrystalline silicon tubes develop, however, observable sodium contamination after being in operation for several months, when the use of sodium-leaching agents is then required. This contamination, developed under strictly controlled production-oriented environments, could be explained by assuming that during tube operation at oxidation temperature sodium arising from external sources reaches the oxidation chamber by diffusion through the tube wall. The contamination source could be located in furnace refractories surrounding the oxidation tube (11). Once the tube wall becomes loaded with sodium above a critical level, evaporation into the oxidation atmosphere starts to predominate. This is a slow process that may take a long time (several months) in continuous operation depending on environmental conditions (18).

Reactions Occurring When Cleaning Fused Silica Tubes

Cleaning of oxidation tubes is a frequent operation in processing facilities. At room temperature, the clean-
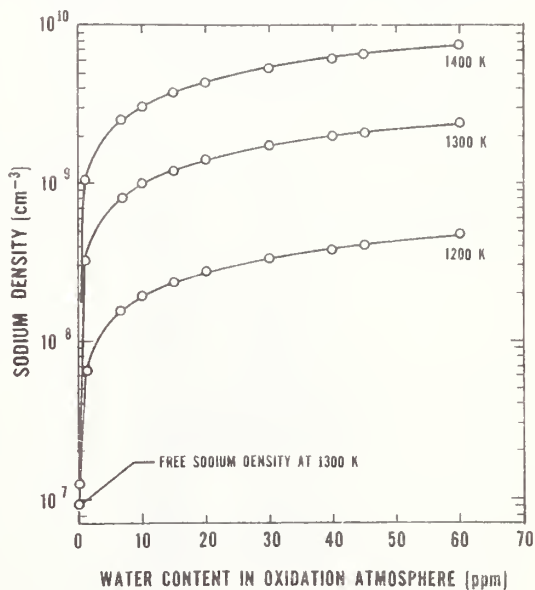

Fig. 1. Total sodium density [cm^{-3}] at equilibrium in fused silica oxidation tube atmosphere as a function of temperature and water impurity. The sodium concentration in silica is assumed 10 ppm, $p(O_2)$ is 1 atm.

Table II. Equilibrium atmosphere in fused silica oxidation tube at 1300°K. Sodium content in fused silica bulk is 10 ppm, oxygen at 1 atm.

Reaction	K	Water content in oxygen: 1 ppm		Water content in oxygen: 30 ppm	
		p (atm)	N (cm^{-3})	p (atm)	N (cm^{-3})
[1] NaO·SiO$_2$ ↔ ½ O$_2$(g) + O(g)	1.76 × 10^{-7}	p(O) = 1.76 × 10^{-7}		p(O) = 1.76 × 10^{-7}	
[2] NaO·SiO$_2$ ↔ NaO(g) + SiO$_2$(c)	7.9 × 10^{-25}	p(NaO) = 7.9 × 10^{-25}		p(NaO) = 7.9 × 10^{-26}	
[3] NaO·SiO$_2$ ↔ 2Na(g) + ½ O$_2$(g) + SiO$_2$(c)	2.5 × 10^{-13}	p(Na) = 1.6 × 10^{-13}	9 × 10^6	p(Na) = 1.6 × 10^{-13}	9 × 10^6
[4] NaO·SiO$_2$ ↔ Na(g) + NaO(g) + SiO$_2$(c)	9.1 × 10^{-20}				
[5] NaO·SiO$_2$ ↔ ¼ O$_2$(g) + 2NaO(g) + SiO$_2$(c)	0.42				
[6] NaO·SiO$_2$ ↔ ¼ O$_2$(g) + 2NaO(g) + SiO$_2$(c)	3.3 × 10^{-20}	p(NaO) = 5.7 × 10^{-15}	3.2 × 10^6	p(NaO) = 5.7 × 10^{-13}	3.2 × 10^6
[7] H$_2$O(g) ↔ H$_2$(g) + ½ O$_2$(g); 2H(g) ↔ H$_2$(g); H$_2$O(g) ↔ H$_2$(g) − OH(g); 2HaO(g) ↔ H$_2$(g) + 2OH(g); H$_2$O(g) ↔ ½ O$_2$(g) + 2OH(g)	1.2 × 10^{-7}; 1.54 × 10^{-14}; 2 × 10$^{-?}$; 2.5 × 10^{-9}	p(H$_2$) = 3 × 10^{-15}; p(H) = 8 × 10^{-14}; p(OH) = 5 × 10^{-8}; p(H$_2$O) = 10^{-4}		p(H$_2$) = 1.7 × 10^{-13}; p(H) = 2.4 × 10^{-13}; p(OH) = 2.7 × 10^{-7}; p(H$_2$O) = 3 × 10^{-3}	
[8] NaO·SiO$_2$(in SiO$_2$) + H$_2$O(g) ↔ 2NaO(g) + H$_2$(g) − SiO$_2$(c)	2.8 × 10^{-7}	p(NaO) = 5.7 × 10^{-15}	3.2 × 10^6	p(NaO) = 5.7 × 10^{-13}	
[9] NaO·SiO$_2$(in SiO$_2$) + H$_2$O(g) ↔ 2NaOH(g) + SiO$_2$(c)	1.5 × 10^{-5}	p(Na$_2$(OH)$_2$) = 1.5 × 10^{-21}		p(Na$_2$(OH)$_2$) = 4.5 × 10^{-15}	
[10] NaO·SiO$_2$(in SiO$_2$) + H$_2$O(g) ↔ 2NaOH(g) + SiO$_2$(c)	3.1 × 10^{-11}	p(NaOH) = 5.6 × 10^{-11}		p(NaOH) = 3 × 10^{-10}	1.7 × 10^6
[11] NaO(g) + H$_2$O(g) ↔ NaOH(g) + OH(g)	4.7				
		Total sodium density: 3.3 × 10^6		Total sodium density: 1.7 × 10^6	

ing can be accomplished using conventional acid solutions. At oxidation temperatures, the cleaning is made in situ by using 5–10% chlorine or hydrogen chloride diluted in an inert gas carrier. This treatment removes sodium contained in the tube inner "skin" down through a convenient depth. A typical cleaning action of this kind requires up to 20 hr of continuous treatment flushing the cleaning gas at about 4 cm^3/sec (0.5 std ft^3/hr). The several reactions taking place during this process are summarized in Table IV.

Reactions [16], [17], and [18] are solved as a simultaneous system. The resulting sodium number density at equilibrium in the tube atmosphere goes to 8.8 × 10^{16} cm^{-3} or a factor 7.3 × 10^9 higher than the equilibrium sodium number density in a dry oxidation atmosphere. Reactions [16], [19], and [20] show similar results due to hydrogen chloride cleaning. The increase in sodium number density with respect to the dry oxidation condition is also in the 10^9 range. Microdroplets of liquid sodium chloride, if formed on the tube wall hot zone, would be removed by the gas stream and transported to a cooler tube zone where sodium chloride precipitates on the wall (sodium chloride melts at 801°C). This "transpiration mechanism" continues while sodium in the hot zone is available for reaction. It should be mentioned that sodium chloride formed in the gas phase is carried down the flushing gas stream and condenses also at the cooler zone where the temperature is appropriate. The cleaning action can be interpreted in terms of relocating sodium in the tube, depleting the hot zone, and enriching the exhaust tube end where the wall temperature is appropriate for condensation.

Stoichiometric equilibria in reactions [17] through [20] require the use of about 1.5g of chlorine or hydrogen chloride per gram of extracted sodium. Assuming that the oxidation tube wall surface is about 4000 cm^2 and the reaction depth in the wall is 10^{-3} cm, the total reacting volume is 4 cm^3 or about 10g fused silica. Assuming 10 ppm sodium content in the fused silica, the amount of sodium reacting is 10^{-4}g which requires the use of 1.5 × 10^{-4}g of chlorine or hydrogen chloride for complete reaction equilibrium. The density of 10% chlorine at 1300°K is 6.74 × 10^{-5} g/cm^3. At 4 cm^3/sec flow, the chlorine mass transported through the oxidation tube is 2.7 × 10^{-4} g/sec. This shows that the reaction rate is regulated by diffusion of sodium in the fused silica. When sodium in the wall bulk diffuses to the wall surface, the reaction with chlorine takes place immediately. In practice, a cleaning period of about 20 hr is used to deplete the tube wall. The longer the cleaning period, the longer the oxidation tube can later be operated under acceptable oxide growing conditions. These calculations indicate that the amount of sodium removed from the fused silica tube wall through chlorine or hydrogen chloride cleaning is substantial and that such cleaning certainly reduces the sodium content in the inner tube wall surface.

Iodine or hydrogen iodide can also be used for in situ oxidation tube cleaning. The relevant reactions taking place are summarized in Table V. Reactions [25] through [28] show the effectiveness of this type of cleaning indicating that iodine or hydrogen iodide could be used instead of chlorine or hydrogen chloride. However, due to economic reasons, the latter are more extensively used in practice. Since thermodynamic data are not available to the desired extent, similar calculations are not presented here for bromine and hydrogen bromide. However bromine should have an intermediate behavior between chlorine and iodine according to the pattern of the members of the halogen family.

Table III. Equilibrium sodium densities in fused silica oxidation ambient at 1300°K. Oxygen at 1 atm.

Compound	Water content in oxygen: 0		Water content in oxygen: 1 ppm		Water content in oxygen: 30 ppm	
	p(atm)	N(cm⁻³)	p(atm)	N(cm⁻³)	p(atm)	N(cm⁻³)
Na	1.8×10^{-12}	9×10^6	1.6×10^{-12}	9×10^6	1.6×10^{-12}	9×10^6
NaO	5.7×10^{-13}	3.2×10^4	5.7×10^{-13}	3.2×10^6	5.7×10^{-13}	3.2×10^5
Na₂O	7.9×10^{-25}	—	7.9×10^{-25}	—	—	—
NaOH	—	—	5.6×10^{-11}	3.2×10^9	3×10^{-10}	1.7×10^9
Na₂(OH)₂	—	—	1.5×10^{-20}	—	4.5×10^{-19}	—
Sodium number density		1.2×10^7		3.3×10^9		1.7×10^9

Table IV. Equilibrium reactions in fused silica tubes at 1300°K when cleaning with 10% Cl₂ or HCl in N₂ carrier at 1 atm.

	Reaction	K	p(atm)	N(cm⁻³)
[12]	Cl₂(g) → 2Cl(g)	1.6×10^{-4}	p(Cl) ≅ 4×10^{-3} p(Cl₂) ≅ 9.6×10^{-2}	
[13]	HCl(g) → H(g) + Cl(g)	1×10^{-13}	p(HCl) ≅ 0.1 p(Cl) ≅ 3.2×10^{-7}	
[14]	HCl(g) → ½ H₂(g) + ½ Cl₂(g)	7.5×10^{-6}	p(Cl₂) = 75×10^{-6}	
[15]	NaCl(l) → NaCl(g)	1.25×10^{-2}	p(NaCl) = 1.25×10^{-2}	(vapor pressure)
[16]	2NaCl(g) → Na₂Cl₂(g)	27.1	p(NaCl) = 1.01×10^{-2}	5.7×10^{16}
[17]	Na₂O · SiO₂ (in SiO₂) + Cl₂(g) → 2NaCl(g) + ½ O₂(g) + SiO₂(c)	6.4	p(Na₂Cl₂) = 2.76×10^{-3}	3.1×10^{16}
[18]	Na₂O · SiO₂ (in SiO₂) + Cl₂(g) → Na₂Cl₂(g) + ½ O₂(g) + SiO₂(c)	174	p(O₂) = 3.9×10^{-3}	
			Sodium number density	6.6×10^{16}
[16]	2NaCl(g) → Na₂Cl₂(g)	27.1	p(NaCl) = 4.1×10^{-3}	2.3×10^{16}
[19]	Na₂O · SiO₂ (in SiO₂) + 2HCl(g) → 2NaCl(g) + H₂O(g) + SiO₂(c)	0.42	p(Na₂Cl₂) = 4.6×10^{-3}	5.2×10^{15}
[20]	Na₂O · SiO₂ (in SiO₂) + 2HCl(g) → Na₂Cl₂(g) + H₂O(g) + SiO₂(c)	11.4	p(H₂O) = 2.5×10^{-3}	
			Sodium number density	2.6×10^{16}

Table V. Equilibrium reactions in fused silica tubes at 1300°K when cleaning with 10% I₂ or HI in N₂ carrier at 1 atm.

	Reaction	K	p(atm)	N(cm⁻³)
[21]	½ I₂(g) → I(g)	0.467	p(I) = 1.0×10^{-1} p(I₂) = 4.5×10^{-2}	
[22]	2HI(g) → H₂(g) + I₂(g)	0.0501	p(I) = 3.57×10^{-2} p(I₂) = 5.6×10^{-3}	
[23]	2HI(g) → H₂(g) + 2I(g)	0.0109	p(H₂) = 2.36×10^{-2} p(HI) = 5.22×10^{-2}	
[24]	NaI(l) → NaI(g)	7.06×10^{-2}	p(NaI) = 7.06×10^{-2}	(vapor pressure)
[25]	Na₂O · SiO₂ (in SiO₂) + I₂(g) → 2NaI(g) + ½ O₂(g) + SiO₂(c)	9.3×10^{-4}	p(NaI) = 9.3×10^{-3} *	
[26]	Na₂O · SiO₂ (in SiO₂) + 2I(g) → 2NaI(g) + ½ O₂(g) + SiO₂(c)	4.3×10^{-4}	Sodium number density	5.3×10^{14}
[27]	Na₂O · SiO₂ (in SiO₂) + 2I(g) + H₂(g) → 2NaI(g) + H₂O(g) + SiO₂(c)	4.9×10^3	p(NaI) = 1.4×10^{-2} *	
[28]	Na₂O · SiO₂ (in SiO₂) + 2HI(g) → 2NaI(g) + H₂O(g) + SiO₂(c)	54.2	Sodium number density	7.9×10^{16}

* p(Na₂I₂) can be estimated about 0.5 p(NaI) from similar results obtained with the chlorine system. No thermodynamic data are available for Na₂I₂.

The Oxidation Atmosphere as a Sodium Contamination Source

An experimental test was made to check the validity of assuming that sodium becomes trapped in an oxidation tube due to the evaporation-transpiration-condensation cycle mentioned above. In a fused silica tube operated at 1000°C "dry" oxygen[5] was allowed to flow at a rate of 4 cm³/sec for 120 hr. The exhaust gas was passed through a 5% hydrochloric acid solution. After this period the solution was analyzed by flame emission spectrometry. The detection limit for sodium in the solution was 10^{-10} g/cm³. No evidence of sodium was detected in the solution after correcting for evaporation of the liquid. This test was repeated twice with consistently negative results. Consequently, it was concluded that sodium is not carried out of the oxidation tube.

There is no apparent way of extracting from a furnace tube a representative sample of the oxidation atmosphere. Other analytical techniques operating on gas samples removed from the oxidation atmosphere, such as mass spectrometry, are not appropriate to detect sodium due to condensation as the temperature decreases. On the other hand, any analytical instrumentation if introduced into the oxidation tube could change the oxidation atmosphere equilibrium adding extra contamination, thus perturbing the measurements.

[5] Electronic grade oxygen typically contains about 5 ppm water and 20 ppm hydrocarbons measured as methane.

Contamination of Thermally Grown Silicon Dioxide Films

The results of Tables I and II indicate that in typical fused silica oxidation tubes the equilibrium atmosphere contains atomic and molecular sodium species resulting in a sodium number density in the 10^7–10^9 cm⁻³ range, depending on the amount of water present. Due to the low density, sodium atoms and molecules contained in the oxidation ambient can be considered as ideal gases. The number of collisions per unit time sodium executes per unit area on the wafer surface is expressed as (19)

$$\nu = 0.25 \, N v$$

where N is the sodium number density in the oxidation atmosphere, $v = (8 \, kT/\pi m)^{1/2}$ is the average molecular velocity at temperature T, k is the Boltzmann constant, and m is the weight of the sodium species. The resulting value of ν for $T = 1300$°K is 10^{12} cm⁻² · sec⁻¹ for $N = 5 \times 10^7$ cm⁻³. The presence of oxygen (1 atm) in the tube slightly modifies this number due to collisions with sodium atoms and molecules.

A number of reactions can take place between the growing silicon dioxide film and the impinging sodium molecules as shown in Table VI. Sodium silicate is formed by reactions [29] through [35] which have high equilibrium constants. As sodium from the oxidation atmosphere becomes incorporated into the oxide

23

Table VI. Impurity reactions with SiO_2 films in fused silica oxidation tube atmospheres at 1300°K

	Reaction	K
[1]	$\frac{1}{2} O_2(g) \rightarrow O(g)$	1.76×10^{-7}
	$H_2(g) \rightarrow 2H(g)$	1.2×10^{-12}
	$H_2O(g) \rightarrow H(g) + OH(g)$	1.54×10^{-11}
[7]	$2H_2O(g) \rightarrow H_2(g) + 2 OH(g)$	2×10^{-16}
	$H_2O(g) \rightarrow H_2(g) + \frac{1}{2} O_2(g)$	2.5×10^{-9}
[29]	$Na_2O(g) + SiO_2(c) \rightarrow Na_2O \cdot SiO_2 \, (\text{in } SiO_2)$	1.3×10^{10}
[30]	$2Na(g) + \frac{1}{2} O_2(g) + SiO_2(c) \rightarrow Na_2O \cdot SiO_2 \, (\text{in } SiO_2)$	4×10^{15}
[31]	$Na(g) + NaO(g) + SiO_2(c) \rightarrow Na_2O \cdot SiO_2 \, (\text{in } SiO_2)$	1.1×10^{10}
[32]	$2NaO(g) + SiO_2(c) \rightarrow Na_2O \cdot SiO_2 \, (\text{in } SiO_2) + \frac{1}{2} O_2(g)$	3×10^{10}
[33]	$2NaO(g) + H_2(g) + SiO_2(c) \rightarrow Na_2O \cdot SiO_2 \, (\text{in } SiO_2) + H_2O(g)$	3.6×10^{26}
[34]	$Na_2(OH)_2 + SiO_2(c) \rightarrow Na_2O \cdot SiO_2 \, (\text{in } SiO_2) + H_2O(g)$	6.7×10^{5}
[35]	$2NaOH(g) + SiO_2(c) \rightarrow Na_2O \cdot SiO_2 \, (\text{in } SiO_2) + H_2O(g)$	3.2×10^{9}

film, more sodium from the tube wall evaporates into the atmosphere, maintaining the equilibrium.

There are not enough kinetic data available to estimate precisely the actual amount of sodium incorporated into the silicon dioxide film during the oxidation cycle. The typical dry oxidation period used to grow a 100 nm thick oxide film on a (100) sample of silicon at 1000°C is about 200 min. During this period the oxide film is subjected to about 10^{16} sodium collisions per square centimeter. Parameters such as the wafer temperature, oxygen flow, and the water content in the tube certainly influence the oxide film contamination level At equilibrium, the sodium concentration in the oxide film grown on silicon should be similar to that in the oxidation tube wall bulk, i.e., 10 ppm ($\sim 10^{17}$ cm^{-3}). This consideration clearly establishes that dry oxidation of silicon made in fused silica tubes produces oxide films with a significant amount of sodium included; the upper limit is determined by the impurity level in the fused silica bulk. Whether or not this sodium which has chemically reacted with silica to form sodium silicate in the film (Table VI) influences the electrical and radiation properties of MOS devices is a matter that needs detailed examination.

It has been reported that structurally included sodium atoms in silicon dioxide films behave like immobile ionic contamination. Capacitance measurements on MOS capacitors with a dielectric of silicon dioxide doped with sodium to density of 10^{20} cm^{-3} showed that most of the included sodium is inactive from the viewpoint of both surface-state density and ionic migration under high electric field at elevated temperature (15). However, instability of semiconductor devices due to sodium mobility in thermal silicon dioxide films has been largely recognized as a central problem in semiconductor technology. Sodium was shown to cause instability under bias-temperature stress in silicon devices made by planar technology. Thermally stimulated ionic conductivity measurements made on MOS capacitors using aluminum or gold as the gate metal have shown that in sodium-doped gate oxide films with surface concentrations in the 10^{11}-10^{13} cm^{-2} range, sodium moves at temperatures above 200°C under electric fields as low as 1.2×10^5 V/cm (20).

In practice instabilities due to sodium can be eliminated either by stringent cleanliness during oxide processing or by the formation of a protective layer such as phosphosilicate glass which can trap sodium (20).

An experimental test was made in a carefully controlled fused silica tube operated at 1000°C and periodically cleaned *in situ* with chlorine. Silicon dioxide films 50-100 nm thick were grown on (100) n-type silicon surfaces using dry electronic grade oxygen and annealed *in situ* after oxidation in dry nitrogen for 30 min. The metal gate was applied by evaporation of 1 μm thick aluminum film in an electron-gun evaporator. MOS capacitors were prepared and capacitance measurements were made at room temperature before and after stressing the capacitors at 300°C for 5 min

with electric field of 10^6 V/cm (2). The results indicate a clear correlation between cleaning of the fused silica oxidation tube and the total mobile ion surface density in the oxide film. These measurements indicate that oxide films grown in recently cleaned tubes show mobile ion densities in the 10^{10} cm^{-2} range.

Assuming uniform contamination film in the measurements, these "clean" oxides exhibit an impurity number density in the 10^{15} cm^{-3} range. This contamination level is caused by impurities accumulated during the device preparation process. It has been shown that radiation sensitivity of gate oxide films has no correlation with the mobile ion content in the oxide as measured by MOS capacitance measurements after bias temperature stressing or high temperature ramping (21) However a correlation of total sodium content with radiation sensitivity in the oxide of various MOS devices has been reported (22). These considerations suggest that sodium contamination introduced in the oxide film during oxidation and metallization may play a prominent role in determining the device radiation resistance. Phosphorus gettering of the gate region or hydrochloric acid passivation increases the radiation sensitivity of MOS devices. Hence to obtain reliable, radiation-stable MOS devices in the absence of gettering it has been suggested that high standards of cleanliness should be maintained (21). This is specially applicable to the oxidation step. Alkali impurity introduced through metallization should also be minimized by careful investigation of the mechanisms through which such contamination is introduced.

Conclusions

The results of the present thermodynamic calculations show that sodium included in the bulk of fused silica oxidation tubes is a significant source of contamination in oxidation atmospheres, even if sodium surface contamination produced by external agents in the tube is negligible. The presence of water in the oxidation atmosphere produces a rapid buildup of the sodium number density from the 10^7 cm^{-3} range, corresponding to dry oxidation, of up to two orders of magnitude greater for water concentrations of a few parts per million. During the oxidation cycle, sodium is incorporated into the oxide film as sodium silicate developing a significant contamination level which can be potentially harmful for MOS device radiation resistance. Water may be incorporated in the oxidation atmosphere through trace water or hydrogen from hydrocarbon impurities included in oxygen, and by ambient water that diffused into the oxidation chamber through the fused silica tube wall.

Preparation of clean oxide films requires the control of sodium impurity in the oxidation atmosphere. This in turn imposes a strict control of the tube material and appropriate care concerning the environmental conditions during wafer processing.

spectrometry. The collaboration of T. F. Leedy and R. Y. Koyama of the Electronic Technology Division in preparing MOS capacitors and in measuring their electrical properties is highly appreciated. This work was conducted as part of the Semiconductor Technology Program at the National Bureau of Standards and was supported in part by the Defense Nuclear Agency (IACRO 76-816) and the NBS.

Manuscript submitted Aug. 3, 1976; revised manuscript received Dec. 20, 1976.

Any discussion of this paper will appear in a Discussion Section to be published in the December 1977 JOURNAL. All discussions for the December 1977 Discussion Section should be submitted by Aug. 1, 1977.

Publication costs of this article were assisted by the National Bureau of Standards.

APPENDIX[6]

Calculation of Equilibrium Reaction Constant from JANAF Data

For a reaction $xX + yY \rightarrow wW + zZ$ the thermodynamic equilibrium constant may be written as

$$K = \frac{\alpha^w(W) \cdot \alpha^z(Z)}{\alpha^x(X) \cdot \alpha^y(Y)}$$

where $\alpha(X)$ is the activity of compound X. For calculations involved in this work (dealing with very dilute gaseous species), the activity may be taken as the partial pressure of the vapor phase (measured in atmospheres). The activity of a solid phase such as $SiO_2(c)$ is taken by convention as unity. For Na_2SiO_3 solid solution in SiO_2 the activity is taken

Table VII. JANAF thermodynamic data used to calculate equilibrium conditions at 1300°K for reactions listed in Tables I–VI

| Compound	$\Delta H°_{f298}$ [*] (kcal/mole)	$-(G°_T - H°_{298})/T$ [**] (cal/°K mole)
$H_2O(g)$	−57.798	51.136
$H(g)$	52.1	30.879
$OH(g)$	9.432	48.677
$O(g)$	59.559	42.044
$O_2(g)$	0	54.283
$H_2(g)$	0	36.130
$Na(g)$	25.755	40.201
$NaOH(g)$	−50.4	63.766
$NaO(g)$	20.0	60.696
$Na_2(OH)_2(g)$	154.6	89.141
$Na_2O \cdot SiO_2$ (in SiO_2)	−376.8†	50.565
$SiO_2(c)$ (quartz)	−217.7	19.918
$Na_2O(g)$‡	8.7	72.3
$HCl(g)$	−22.063	49.624
$Cl_2(g)$	0	59.316
$Cl(g)$	28.922	43.228
$NaCl(g)$	−43.36	61.099
$NaCl(l)$	−92.237	32.199
$NaCl(c)$	−96.26	26.479
$Na_2Cl_2(g)$	−135.3	91.387
$I(g)$	25.537	46.671
$I_2(g)$	14.924	68.559
$HI(g)$	6.3	54.425
$NaI(g)$‡	−22.7	64.8
$NaI(l)$	−63.695	36.532
$NaI(c)$	−88.6	32.656

[*] $\Delta H°_{f298}$ = standard enthalpy of formation.
[**] $(G°_T - H°_{298})/T$ = Gibbs energy function in the standard state at temperature 1300°K
† The value of $\Delta H°_{f298}$ for $Na_2O \cdot SiO_2$ (in SiO_2) was calculated using the equilibrium constant from reaction [3] Table I [see Ref. (12)]. The free energy function was assumed to be that of $Na_2O \cdot SiO_2$ (gls) given by the JANAF tables.
‡ The Na_2O data were estimated from various lithium, sodium, and potassium oxidea data given in the JANAF tables. The NaI data are likewise estimated using the available alkali halide data.

as the mole fraction (10^{-5} in the present work) For the reaction

$$Na_2O \cdot SiO_2(gls) + \tfrac{1}{2}O_2(g) \rightarrow 2NaO(g) + SiO_2(c)$$
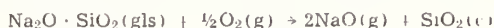
the equilibrium constant is expressed as

$$K = p^2(NaO) \times 10^5/p^{1/2}(O_2)$$

To evaluate K at a particular temperature T (measured in Kelvin) the following relations are used

$$\Delta G_T = -RT \ln K$$

$$\Delta G_T = \Delta H°_{298} + T(\Sigma(G°_T - H°_{298})/T)$$

where $\Delta H°_{298}$ is the heat of reaction, calculated from standard heats of formation as

$$\Delta H°_{f298} = \Sigma \Delta H°_{f298}(products) - \Sigma \Delta H°_{f298}(reactants)$$

[kcal/mole]

and $\Sigma(G°_T - H°_{298})/T$ is calculated from Gibbs energy function in the standard state at temperature T

$$\Sigma(G°_T - H°_{298})/T = \{\Sigma(G°_T - H°_{298})/T\}_{products}$$

$$- \{\Sigma(G_T - H_{298})/T\}_{reactants} \quad [cal/°K mole]$$

[6] This calculation follows standard thermodynamic formalism [see Ref (23)]

REFERENCES

1. S. Schlegal, *IEEE Trans Electron Devices*, **ed-14**, 728 (1967); *ibid.*, **ed-15**, 951 (1968)
2. K. H Zaininger, *RCA Rev.*, **27**, 341 (1966).
3. R. J. Kriegler, "12th Annual Proceedings, Reliability Physics 1974," IEEE Catalog No 74CHO839-1 PHY, pp. 250–258 (1974)
4. B. Yurash and B Deal, *This Journal*, **115**, 1191 (1968).
5. W. R. Knolle, *ibid.*, **120**, 987 (1973)
6. W. R. Knolle and T F. Retajczyk, Jr, *ibid.* **120**, 1106 (1973).
7. K. G. Aubuchon, *IEEE Trans Nucl Sci.*, **ns-18**, No. 6. 117 (1971)
8. G. Hetherington, G W. Stephenson, and J A. Winterburn, *Electronic Eng.*, **41**, No 495, 52 (1969). *ibid.*, **41**, No. 496, 44 (1969)
9. A E. Owen and R. W Douglas. *J Soc Glass Technol.*, **43**, 159T (1959).
10. H. F. Wolf, "Silicon Semiconductor Data," pp 526-527, Pergamon Press, Oxford (1969)
11. D. R. Fewer and W. L. Gill, Tech Rep. No. RADC-TR-66-345, pp. 33–49 (1966); also available as NTIS Document AD-489-969
12. G. L. Vidale, General Electric Co, Technical Information Series, R60SD390 (1960)
13. JANAF Thermochemical Tables D R Stull and H. Prophet, Editors, 2nd ed. NSRDS-NBS 37 (1971).
14. E. A. Irene, *This Journal*, **121**, 1613 (1974)
15. A. G. Revesz and R. J. Evans, *J. Phys Chem Solids*, **30**, 551 (1969).
16. S. Mayo, R. A. Keller, J. C. Travis, and R. B Green, *J. Appl. Phys.*, **47**, 4012 (1976).
17. W. Dietze, L. P. Hunt, and D. H Sawyer, *This Journal*, **121**, 1112 (1974).
18. D H. Sawyer, Private communication.
19. S. Dushman, "Scientific Foundations of Vacuum Technique," 2nd ed., p. 14, John Wiley & Sons, Inc., New York (1962).
20. T. W. Hickmott, *Appl. Phys Lett.*, **22** 267 (1973); *Phys. Rev. Lett.*, **32**, 65 (1974), *J. Appl. Phys.*, **46**, 2583 (1975)
21. B. L. Gregory, *IEEE Trans. Nucl Sci.*, **ns-22**, No. 6. 2295 (1975).
22. H. Hughes, R. D. Baxter, and B. Phillips, *ibid.*, **ns-19**, No. 6, 256 (1972).
23. G N. Lewis and M. Randall, "Thermodynamics," 2nd ed., chap. 15, McGraw Hill Book Co., New York (1961).

Appendix 3

Thermodynamic Considerations in the Use of Polysilicon Oxidation Tubes for Clean SiO₂ Film Preparation

Santos Mayo*

*National Bureau of Standards, Electronic Technology Division,
Institute for Applied Technology, Washington, D.C. 20234*

and William H. Evans

*National Bureau of Standards, Physical Chemistry Division,
Institute for Materials Research, Washington, D.C. 20234*

ABSTRACT

The thermodynamic equilibria established in oxidation atmospheres in polycrystalline silicon tubes operated at 1000°C are analyzed. Silicon oxidation tubes made by chemical vapor deposition through hydrogen reduction of pure trichlorosilane have very low sodium content (about 10 ppb or 1000 times less sodium than in transparent fused silica oxidation tubes). Due to the low sodium content in new oxidation tubes, clean (low alkali content) thermal oxide films can be grown on silicon wafers. However, tube contamination developed during semiconductor processing operations imposes the need for appropriate periodic tube cleaning to maintain sodium contamination in the oxidation atmosphere within acceptable levels. Tube cleaning reactions taking place at oxidation temperature are discussed showing that the quality of thermal oxide films is influenced by tube cleaning efficiency.

Preparation of thermally grown clean oxide films on silicon wafers has great technological impact on successful microelectronic device fabrication. Although

the understanding of the role played by alkali ions in such films is not complete, especially concerning the behavior of electrically "active" and "inactive" contamination (1), the presence of alkali species in thermally grown silicon dioxide films has been ex-

27

perimentally demonstrated to cause ionic conductivity and consequently instabilities in metal-oxide semiconductor (MOS) devices (2-5). The presence of sodium and other alkali species in thermally grown oxide films used for semiconductor device preparation has been extensively investigated (6-8). Sources of alkali contamination have also been investigated in processing materials (9-13), in oxidation furnace refractories (14), and in evaporated gate metal films (15). Addition of about 5% chlorine or hydrogenchloride to the oxidation atmosphere has been reported to enhance the electrical stability of Si-SiO$_2$ structures, both through cleaning and passivating effects (16-22). HCl diluted in an inert gas carrier (concentration up to 10%) is used for periods of several hours immediately before oxidations to produce low mobile-ion content thermal oxide films for MOS device fabrication.

In a recent paper (23) the development of sodium contamination in oxidation atmospheres contained in transparent fused silica tubes operated at 1000°C was analyzed thermodynamically in terms of the impurity content primarily included in fused silica bulk resulting from the tube manufacturing process. Transparent fused silica tubes currently used in most semiconductor processing furnaces contain about 10 ppm sodium (24-25). *In situ* cleaning of fused silica tubes at 1300°K results in removal of material from the inner tube wall surface creating a sodium-depleted layer. This in turn reduces the sodium content in the oxidation ambient, allowing the thermal growth of cleaner oxide films on silicon wafers. However, due to its high diffusivity in SiO$_2$ [$D = 2 \times 10^{-6}$ cm^2/sec at 1000°C (26)] sodium from furnace refractories or from the room atmosphere around the oxidation tube may be incorporated into the fused silica wall contributing to the maintenance of its contamination level. When fused silica oxidation tubes are replaced by silicon tubes, the conditions established in the oxidation ambient are expected to be more favorable for growing clean thermal oxide films on silicon wafers. This is caused by the low sodium content in silicon tubes fabricated by chemical vapor deposition through hydrogen reduction of trichlorosilane. This process produces high purity polysilicon with only 10 ppb sodium contamination, 1000 times less sodium content than in fused silica tubes (28). However, due to external contamination sources (i.e., sodium from refractories and room ambient), periodic *in situ* cleaning of the tube is necessary to maintain appropriate conditions in the oxidation atmosphere. The cleaning interval for both fused silica or silicon tubes is determined by the boundary conditions at the tube wall outer surface and the diffusion of sodium in the tube

wall. The diffusion coefficient of sodium in polycrystalline silicon is higher than in single crystal silicon due to grain boundary effects. At 1000°C the latter is $D = 3 \times 10^{-6}$ cm^2/sec (26). Similar effects were reported on the diffusion of boron in silicon at 1050°C (27).

The work presented here is an extension of the previous analysis on the behavior of fused silica oxidation tubes at 1000°C (23).[1] Silicon oxidation tube behavior resembles the fused silica tube behavior except for the initial low sodium content when the tube is new. The effects of HCl cleaning on these tubes are also analyzed.

Oxidation of Silicon Wafers in Silicon Oxidation Tubes

The kinetics of silicon oxidation have been extensively studied by different authors for a number of temperatures in the range of 800°-1200°C and for several oxidation atmosphere compositions contained in fused silica tubes [most early work on this subject is listed in bibliographic compilations on MOS technology (9, 30)]. It was shown that the addition of trace amounts of water to the oxidation ambient causes a significant increase of silicon oxidation rate for all silicon orientations (31). It has also been shown that the equilibrium sodium density in oxidation atmospheres at 1300°K significantly increases when a few ppm water are added to the oxidation atmosphere (23). From these results it can be stated that the preparation of clean, low mobile ion content oxide films on silicon wafers is controlled primarily by four parameters: the oxidation temperature, the amount of sodium (in general, alkali) contamination in the tube wall bulk, the amount of water content in the oxidation atmosphere, and the furnace environment. The use of strictly controlled hydrocarbon-free dry oxygen in addition to alkali-free oxidation tubes operated at high temperatures (above 1000°C) may result in clean thermal oxide preparations if appropriate care is taken concerning clean room environments around oxidation facilities. For high temperature (close to 1200°C) processes where devitrification of fused silica may produce serious problems, silicon tubes are preferred due to their better mechanical behavior and low sodium contamination level.

In the present work, the equilibrium atmosphere established at 1300°K in a silicon oxidation tube was studied theoretically for a number of cases of practical interest.[2] Table I shows the equilibrium atmo-

[1] For these thermodynamic calculations data at 1300°K are used.
[2] The scheme for these calculations is outlined in the appendix of Ref. 23. Because of errors and approximations involved in the thermodynamic data used to evaluate the equilibrium results, an absolute error of ±50% could be expected in these calculations. The relative error is much smaller.

Table I. Equilibrium atmosphere in silicon wet oxidation tube at 1300°K

Sodium content in silicon bulk: 10 ppb, oxygen at 1 atm, water at 10⁻⁴ atm

Reaction	K	Product	P (atm)	Na(cm⁻³)
Si(c) + O$_2$(g) + H$_2$O(g) → SiO$_2$(c) + ½H$_2$(g) + OH(g)	2.54 × 10^{19}	O$_2$	1.0	
2H$_2$(g) + O$_2$(g) → 2H$_2$O(g)	1.35 × 10^{11}	H$_2$(g)	8.61 × 10^{-14}	
Si(c) + O$_2$(g) → SiO$_2$(c)	1.8 × 10^{27}*	OH	4.82 × 10^{-7}	
SiO(g) + ½ O$_2$(g) → SiO$_2$(c)	5.59 × 10^{19}	H$_2$O	10^{-4}	
Na$_2$O · SiO$_2$(c) → SiO$_2$(c) + Na$_2$O(g)	7.83 × 10^{-20}	Na$_2$O	7.9 × 10^{-29}	
Na$_2$O · SiO$_2$(c) + H$_2$O → SiO$_2$(c) + 2Na(g) + 2 OH(g)	5.85 × 10^{-78}	Na	5.02 × 10^{-14}	
Na$_2$O · SiO$_2$(c) + H$_2$O → SiO$_2$(c) + Na$_2$O(g) + OH(g)	1.19 × 10^{-30}	SiO(OH)	3.13 × 10^{-15}	
Na$_2$O · SiO$_2$(c) + H$_2$O → Si(OH)$_2$(g) + ½ O$_2$(g) + Na$_2$O(g)	1.68 × 10^{-42}	Si(OH)$_2$	2.13 × 10^{-23}	
Na$_2$O · SiO$_2$(c) + H$_2$O → SiO(OH)$_2$(g) + Na$_2$O(g)	2.72 × 10^{-28}	SiO(OH)$_2$	3.44 × 10^{-17}	
Na$_2$O · SiO$_2$(c) + 2H$_2$O → Si(OH)$_4$(g) + Na$_2$O(g)	1.57 × 10^{-27}	Si(OH)$_4$	2.00 × 10^{-16}	
2Na$_2$O · SiO$_2$(c) + 3H$_2$O → Si$_2$O(OH)$_6$(g) + 2Na$_2$O(g)	1.38 × 10^{-51}	Si$_2$O(OH)$_6$	2.21 × 10^{-30}	
Si(c) + 2H$_2$O(g) → SiO$_2$(c) + 2H$_2$(g)	1.33 × 10^{12}			
Si(c) + H$_2$O(g) → SiH(g) + OH(g)	5.19 × 10^{-15}	SiH	1.08 × 10^{-16}	
Si(c) + 2H$_2$O(g) → SiH$_4$(g) + O$_2$(g)	8.00 × 10^{-21}	SiH$_4$	8.00 × 10^{-20}	
Si(c) + 3/2 O$_2$(g) + 2Na(g) → Na$_2$O · SiO$_2$(c)	7.14 × 10^{46}			
Si(c) + 5/2 O$_2$(g) + 2Na(g) → Na$_2$O · 2SiO$_2$(c)	1.21 × 10^{73}			
Na$_2$O · SiO$_2$(c) + SiO$_2$(c) → Na$_2$O · 2SiO$_2$(c)	0.944			
Na$_2$O(g) + ½ O$_2$(g) → 2NaO(g)	0.42	NaO	1.82 × 10^{-14}	
Na$_2$O(g) + H$_2$O(g) → NaOH(g) + OH(g)	4.69	NaOH	1.77 × 10^{-13}	9.99 × 10^7 ≈10^8
2NaOH(g) → Na$_2$(OH)$_2$(g)	4.78	Na$_2$(OH)$_2$	1.50 × 10^{-21}	

* Rapid formation of a silica film on the silicon tube.

sphere resulting in a typical silicon oxidation tube operated at 1300°K using pure oxygen at 1 atm plus 100 ppm water. Sodium in the tube wall might be assumed to be sodium metasilicate $[Na_2O \cdot SiO_2(c)]$ and sodium silicate $[Na_2O \cdot 2SiO_2(c)]$. Measurements of sodium vaporization from silica glasses (32) indicate that sodium metasilicate might be dominant; deviations of the value $\Delta H°_{f298} = -376.8$ kcal/mole calculated for $Na_2O \cdot SiO_2(c)$ from the JANAF value (33) is ascribed to solution effects of $Na_2O \cdot xSiO_2$ species. Silicon and water react to form $SiO_2(c)$ (equilibrium reaction constant $K = 1.33 \times 10^{13}$). Sodium metasilicate is incorporated in the oxide film developed on the tube wall and evaporates to build up in the oxidation chamber an atmosphere containing about 10^8 sodium atoms/cm^3, including both atomic and molecular species; NaOH is the most abundant compound. If no water is present in the oxidation ambient, the sodium content is negligible $[P(Na_2O) = 7.9 \times 10^{-28}$ atm]. This condition prevails as long as the sodium level in silicon bulk is only 10 ppb.

Oxidation Tube Cleaning

Periodic *in situ* cleaning at oxidation temperature is required to keep silicon oxidation tubes clean under operative conditions. Dilute hydrogen chloride is generally used for rather long periods in the oxidation chamber to assure proper cleaning of the wall. Assuming 100 ppm water (10^{-4} atm) in addition to 10% HCl in a silicon tube operated at 1300°K, the relevant reactions occurring are shown in Table II. Sodium chloride is formed from the interaction with sodium glasses contained in the silica film formed on the silicon tube wall. At equilibrium, the sodium number density in the atmosphere is 3.66×10^{15} atoms/cm^3. This is 10^7 times larger than the equilibrium sodium density normally present in the oxidation ambient. It should be emphasized that these results refer to equilibrium conditions. Although most reactions proceed rapidly at the inner tube wall surface, diffusion effects in the bulk may limit to some extent the applicability of this analysis. However, the enhanced sodium diffu-

sion in polysilicon will reduce this limitation. The density of the resulting species at the surface could be lower, thus reducing the amount of sodium (or other species) actually removed. No attempts are made here to explore the kinetics of these reactions although it can be seen that hydrogen chloride cleaning is predicted to be very effective in agreement with current empirical observation.

The use of dry chlorine as a cleaning agent of silicon tubes should be avoided because of the risk involved due to its high reactivity with silicon. Table III shows that the tube could be severely damaged by chlorine if the protective silica film deposited on the inner tube wall has pinholes through which chlorine may come in contact with silicon to produce quantities of $SiCl_4(g)$, $SiCl_3(g)$, and $SiCl_2(g)$. However, if water is present in the system, hydrogen chloride is generated, moderating the aggressive behavior of dry chlorine.

Oxidation Tube Conditioning

The silica film formed on the tube wall can be removed by hydrogen at oxidation temperature. The formation of water generated through the hydrogen silica interaction contributes to the leaching of sodium from the tube bulk. Table IV shows the relevant reactions taking place in the tube when 100 ppm water (10^{-4} atm) is present in the hydrogen atmosphere. Sodium compounds such as NaO, Na_2O, NaOH, and $Na_2(OH)_2$ are formed in addition to atomic sodium. The total sodium equilibrium pressure in the tube atmosphere is 1.82×10^{-8} atm resulting in a number density of 1.03×10^{11} atoms/cm^3 where the atomic species is the most abundant one due to the reducing action of hydrogen. Although the use of hydrogen around an oxidation facility involves risks and difficulties which may make it impractical, it is of value to observe that the use of diluted (less than 4%) hydrogen in an inert gas carrier could make this procedure feasible by eliminating the risk of forming an explosive air-hydrogen mixture. If such an atmosphere is maintained in silicon oxidation tubes when they are

Table II. Equilibrium atmosphere in silicon oxidation tube cleaned with hydrogen chloride at 1300°K

Sodium content in silicon bulk: 10 ppb, hydrogen chloride at 0.1 atm, water at 10^{-4} atm

Reaction	K	Product	P (atm)	Na (cm^{-3})
$Na_2O \cdot SiO_2(c) + 2HCl(g) \rightarrow SiO_2(c) + 2NaCl(g) + H_2O(g)$	0.42	NaCl	6.48×10^{-4}	3.66×10^{15}
$Na_2O \cdot SiO_2(c) + 2HCl(g) \rightarrow Si(OH)_2(g) + 2NaCl(g) + \frac{1}{2}O_2(g)$	9.03×10^{-24}	$Si(OH)_2$	1.66×10^{-15}	
$Na_2O \cdot SiO_2(c) + 2HCl(g) \rightarrow SiO(OH)(g) + 2NaCl(g) + OH(g)$	6.39×10^{-18}	SiO(OH)	8.45×10^{-11}	
$Na_2O \cdot SiO_2(c) + 2HCl(g) + H_2O(g) \rightarrow Si(OH)_4(g) + 2NaCl(g)$	8.45×10^{-9}	$Si(OH)_4$	2.01×10^{-12}	
$2Na_2O \cdot SiO_2(c) + 4HCl(g) + 1H_2O(g) \rightarrow Si_2O \cdot (OH)_6(g) + 4NaCl(g)$	3.98×10^{-14}	$Si_2O(OH)_6$	2.26×10^{-21}	
$Na_2O \cdot SiO_2(c) + 3HCl(g) \rightarrow SiCLH_3(g) + 3/2 O_2(g) + 2NaCl(g)$	4.98×10^{-34}	$SiClH_3$	5.50×10^{-14}	
$Na_2O \cdot SiO_2(c) + 4HCl(g) \rightarrow SiCl_2H_2(g) + 1 O_2(g) + 2NaCl(g) + H_2O(g)$	7.38×10^{-29}	$SiCl_2H_2$	1.05×10^{-12}	
$Na_2O \cdot SiO_2(c) + 5HCl(g) \rightarrow SiCl_3H(g) + \frac{1}{2}O_2(g) + 2NaCl(g) + 2H_2O(g)$	3.53×10^{-19}	$SiCl_3H$	6.51×10^{-9}	
$Na_2O \cdot SiO_2(c) + 5HCl(g) \rightarrow SiCl_3(g) + OH(g) + 2NaCl(g) + 2H_2O(g)$	4.14×10^{-20}	$SiCl_3$	5.48×10^{-8}	
$Na_2O \cdot SiO_2(c) + 4HCl(g) \rightarrow SiCl_2(g) + \frac{1}{2}O_2(g) + 2NaCl(g) + 2H_2O(g)$	5.38×10^{-21}	$SiCl_2$	9.91×10^{-10}	
$Na_2O \cdot SiO_2(c) + 6HCl(g) \rightarrow SiCl_4(g) + 2NaCl(g) + 3H_2O(g)$	3.80×10^{-11}	$SiCl_4$	9.04×10^{-7}	
$2NaCl(g) \rightarrow Na_2Cl_2(g)$	27.1	Na_2Cl_2	1.14×10^{-5}	6.43×10^{13}
$Si(c) + HCl(g) \rightarrow SiCl_4(g) + 2H_2(g)$	1.20×10^3	$Si(OH)_2$	1.67×10^{-15}	
$SiO_2(c) + H_2O(g) \rightarrow Si(OH)_2 + \frac{1}{2}O_2(g)$	2.15×10^{-13}	O_2	1.67×10^{-16}	
$H_2O(g) + Cl_2(g) \rightarrow 2HCl + \frac{1}{2}O_2$	1.29×10^{27}	HCl	0.1	
$HCl(g) \rightarrow \frac{1}{2}H_2(g) + \frac{1}{2}Cl_2(g)$	7.5×10^{-5}	Cl_2	9.19×10^{-9}	
$HCl(g) \rightarrow H(g) + Cl(g)$	1.0×10^{-12}	Cl	1.17×10^{-6}	
$H_2(g) \rightarrow 2H(g)$	1.2×10^{-12}	H	8.57×10^{-8}	
$H_2O(g) \rightarrow H(g) + OH(g)$	1.54×10^{-14}	H_2	6.12×10^{-3}	
$2H_2O(g) \rightarrow H_2(g) + 2 OH(g)$	2.0×10^{-16}	OH	1.80×10^{-11}	
$H_2O(g) + \frac{1}{2}O_2(g) \rightarrow 2 OH(g)$	2.5×10^{-9}	H_2O	10^{-4}	

Table III. Reaction constants resulting in silicon oxidation tubes cleaned with chlorine at 1300°K

Sodium content in silicon bulk: 10 ppb, chlorine at 0.1 atm

Reaction	K	Product	P (atm)
$Si(c) + 2Cl_2(g) \rightarrow SiCl_4(g)$	3.77×10^{19}	$SiCl_4$	3.77×10^{17}*
$2Si(c) + 3Cl_2(g) \rightarrow 2SiCl_3(g)$	4.74×10^{-29}	$SiCl_3$	6.91×10^{12}*
$Si(c) + Cl_2(g) \rightarrow SiCl_2(g)$	3.50×10^8	$SiCl_2$	3.50×10^7
$SiO_2(c) + 2Cl_2(g) \rightarrow SiCl_4(g) + O_2(g)$	2.11×10^{-5}		
$2SiO_2(c) + 3Cl_2(g) \rightarrow 2SiCl_2(g) + 2 O_2(g)$	1.48×10^{-36}		
$SiO_2(c) + Cl_2(g) \rightarrow SiCl_2 + O_2(g)$	1.96×10^{-19}		
$Na_2O \cdot SiO_2(c) + Cl_2(g) \rightarrow SiO_2(c) + 2NaCl(g) + \frac{1}{2}O_2(g)$	8.43		

* Rapid formation of these compounds.

Table IV. Equilibrium atmosphere in silicon oxidation tube cleaned with wet hydrogen at 1300°K

Sodium content in silicon bulk. 10 ppb, hydrogen at 1 atm, water at 10^{-4} atm

Reaction	K	Product	P (atm)	Na (cm^{-3})
$SiO_2(c) + H_2(g) + H_2O(g) \rightarrow SiH(g) + 3 OH(g)$	7.86×10^{-11}	SiH	2.80×10^{-16}	
$SiO_2(c) + 2H_2(g) \rightarrow SiH_2(g) + O_2(g)$	6.00×10^{-51}	SiH$_2$	9.38×10^{-17}	
$Na_2O \cdot SiO_2(c) + H_2(g) \rightarrow SiH(g) + OH(g) + O_2(g) + 2Na(g)$	8.43×10^{-90}	Na	1.82×10^{-9}	1.03×10^{11}
$Na_2O \cdot SiO_2(c) + H_2(g) \rightarrow SiH(g) + OH(g) + 2NaO(g)$	1.10×10^{-70}	NaO	5.28×10^{-20}	
$Na_2O \cdot SiO_2(c) + 5/2H_2(g) \rightarrow SiH(g) + H_2O(g) + 2NaOH(g)$	8.49×10^{-33}	NaOH	7.74×10^{-11}	
$Si(c) + H_2O(g) \rightarrow SiO_2(c) + 2H_2(g)$	1.33×10^{15}			
$2NaOH(g) \rightarrow Na_2(OH)_2(g)$	4.78	Na$_2$(OH)$_2$	1.45×10^{-21}	
$Na_2O(g) \rightarrow NaO(g) + Na(g)$	1.16	Na$_2$O	8.28×10^{-30}	
		H$_2$	1.0	
		H$_2$O	10^{-4}	
$2H_2O \rightarrow H_2(g) + 2 OH(g)$	2.0×10^{-13}	OH	1.41×10^{-12}	
$H_2O(g) + \frac{1}{2} O_2(g) \rightarrow 2 OH(g)$	2.5×10^{-9}	O$_2$	6.40×10^{-35}	

Table V. JANAF thermodynamic data used to calculate equilibrium conditions at 1300 K for reactions listed in Tables I-IV

Compound	ΔH°_{298} (kcal/mole)	$(G^\circ_T - H^\circ_{298})/T$ (cal/°K mole)
H$_2$O(g)	-57.798	51.136
H(g)	52.1	30.879
OH(g)	9.432	48.877
O(g)	59.559	42.044
O$_2$(g)	0.0	54.283
H$_2$(g)	0.0	38.130
Na(g)	25.755	40.201
NaOH(g)	50.4	63.186
NaO(g)	20.0	60.896
Na$_2$(OH)$_2$(g)	154.8	89.141
Na$_2$O · SiO$_2$(gls)^c	-376.8	50.565
Na$_2$O · 2SiO$_2$(c)	-590.36	73.554
SiO$_2$(c) (quartz)	-217.7	19.918
Na$_2$O(g)^d	8.7	72.30
HCl(g)	22.063	49.624
Cl$_2$(g)	0.0	59.318
Cl(g)	28.922	43.228
NaCl(g)	43.38	81.099
NaCl(liq)	92.237	32.199
NaCl(c)	-98.28	26.479
Na$_2$Cl$_2$(g)	-135.3	91.387
Si(g)	107.7	43.715
Si(l)	11.585	15.188
Si(c)	0.0	8.399
SiH(g)	90.0	52.515
SiH$_2$(g)	7.3	58.969
SiO(g)	-24.0	55.994
SiO$_2$(g)	73.0	63.266
SiO$_2$(l)	215.74	21.134
SiCl(g)	45.7	62.985
SiClH$_3$(g)	48.0	71.412
SiCl$_2$(g)	-157.1	95.763
SiCl$_2$H$_2$(g)	-75.0	81.596
SiCl$_3$H(g)	119.8	89.722
SiCl$_4$(g)	39.3	76.581
SiCl$_3$(g)^c	98.0	89.134
SiO · (OH)^c	118.0	73.63
Si · (OH)^c	101.0	74.42
SiO · (OH)$_2^c$	222.0	82.65
Si · (OH)$_2^c$	322.3	95.43
SiO$_2$ · (OH)$_2^c$	812.1	132.83

ΔH°_{298} = standard enthalpy of formation.
$(G^\circ_T - H^\circ_{298})/T$ = Gibbs energy function in the standard state at 1300°K.
^{c} The value of ΔH for Na$_2$O · SiO$_2$ (in SiO$_2$) was calculated using the equilibrium constant from reaction Na$_2$O · SiO$_2$(c) → 2Na(g) + $\frac{1}{2}$ O$_2$(g) + SiO$_2$(c), $K = 25 \times 10^{-81}$ (see Ref (32)). The free energy function was assumed to be that of Na$_2$O · SiO$_2$ (gls) given by the JANAF tables.
^{d} The Na$_2$O data were estimated from various lithium, sodium, and potassium oxides data given in the JANAF tables.
^{e} The heats of formation were calculated from bond energies as outlined in Ref (36). The thermodynamic functions were obtained by interpolation of the values given there.

not being used for semiconductor processing, the sodium impurity from the tube wall bulk and the silica film on the tube are constantly removed from the hot zone. The enhanced sodium diffusion in polysilicon increases the sodium migration into the silica film which is being removed by the hydrogen reducing action. This tube conditioning would reduce the need for periodic HCl cleaning and consequently minimize the incidence of other species (such as chlorine) in the oxidation chamber. Experimental evidence shows that chlorine is incorporated into oxide films thermally grown on silicon wafers processed in oxidation tubes previously cleaned with HCl (34). This has proved to be detrimental for radiation-hard devices resulting in electrical instabilities (35).

Conclusions

The above results show that the dominant factor in the preparation of clean thermal oxides is the purity of the oxidation tube wall if other process steps are kept under strict control. Such processes involve the wafer cleaning and handling prior to oxidation and metallization immediately after oxidation. When recently installed, new silicon tubes have a low sodium content and thus constitute an excellent material to enclose the oxidation atmosphere. This is due to the tube fabrication process (chemical vapor deposition) employing highly purified (low alkali) materials (28). Preparation of clean low mobile ion content thermal oxide films by wet oxidation of silicon wafers is in principle possible if silicon oxidation tubes are used, provided that the tube environment is clean enough to avoid inclusion of ambient contamination in the tube. However, a silicon oxidation tube will tend to develop alkali contamination during normal operation unless special care is taken to isolate it from external contamination. These conditions are hard to maintain even in clean production-oriented facilities, so periodic in situ tube cleaning is required. At oxidation temperatures sodium deposited on the exterior of the tube diffuses through the wall into the oxidation atmosphere contaminating the thermal oxide films grown on silicon wafers. The contamination process may be originated by the furnace refractories impurity, the room ambient, and other factors external to the tube. The main advantage of employing silicon oxidation tubes lies in the possibility of using temperatures higher than tolerated by fused silica tubes.

Acknowledgment

REFERENCES

1. B. E. Deal, *This Journal*, 121, 198C (1974)
2. T. W. Hickmott, *J. Appl. Phys.*, 46, 2583 (1975)
3. C. M. Osburn and S. I. Raider, *This Journal*, 120, 1369 (1973)
4. T. H. DiStefano and J. E. Lewis, *J. Vac. Sci. Technol.*, 11, 1020 (1974)
5. G. F. Derbenwick, *J. Appl. Phys.*, 48, 1127 (1977)
6. K. G. Aubuchon, *IEEE Trans. Nucl. Sci.*, NS-18, No. 6, 117 (1971).

7. E. H. Snow, A. S. Grove, B. E. Deal, and C. T. Sah, *J. Appl. Phys.*, **36**, 1664 (1965).
8. B. E. Deal, NBS Special Publication 337, Silicon Device Processing, C. P. Marsden, Editor, pp. 36-50, Washington, D.C. (1970).
9. S. I. Raider, L. V. Gregor, and R. Flitsch, *This Journal*, **120**, 425 (1973).
10. B. Yurash and B. E. Deal, *ibid.*, **115**, 1191 (1968).
11. J. E. Barry, H. M. Donega, and T. E. Burgess, *ibid.*, **116**, 257 (1969).
12. W. R. Knolle, *ibid.*, **120**, 987 (1973).
13. W. R. Knolle and T. F. Retajczyk, Jr., *ibid.*, **120**, 1106 (1973).
14. D. R. Fewer and W. L. Gill, Technical Report No. RADC-TR-66-345, pp. 33-46 (1966); also available as NTIS Document AD-489-969.
15. K. G. Aubuchon, Hughes Research Laboratories Final Tech. Rep., contract N00014-71-C-0079 (1971).
16. R. J. Kriegler, *Appl. Phys. Lett.*, **20**, 449 (1972).
17. R. J. Kriegler, Y. C. Cheng, and D. R. Colton, *This Journal*, **119**, 388 (1972).
18. R. J. Kriegler, *Thin Solid Films*, **13**, 11 (1972).
19. R. J. Kriegler, in "Semiconductor Silicon 1973," H. R. Huff and R. R. Burgess, Editors, p. 363, The Electrochemical Society Softbound Symposium Series, Princeton, N.J. (1973).
20. R. J. Kriegler, in "12th Annual Proceedings Reliability Physics 1974," IEEE Catalog No. 74CHO-839-1PHY (1974).
21. A. Rohatgi, S. R. Butler, and F. J. Feigl, *Appl. Phys. Lett.*, **30**, 104 (1977).
22. Y. J. van der Meulen, C. M. Osburn, and J. F. Ziegler, *This Journal*, **122**, 284 (1975).
23. S. Mayo and W. H. Evans, *ibid.*, **124**, 780 (1977).
24. G. Hetherington, G. W. Stephenson, and J. A. Winterburn, *Electronic Engin.*, **41**, No. 495, 52 (1969); *ibid.*, **41**, No. 496, 44 (1969).
25. A. E. Owen and R. W. Douglas, *J. Soc. Glass Technol.*, **43**, 159T (1969).
26. H. F. Wolf, "Silicon Semiconductor Data," pp. 136-137, 526-527 Pergamon Press, Oxford (1969).
27. S. Horiuchi and R. Blanchard, *Solid-State Electron.*, **SC-18**, 529 (1975).
28. W. Dietze, L. P. Hunt, and D. H. Sawyer, *This Journal*, **121**, 1112 (1974).
29. E. S. Schlegel, *IEEE Trans. Electron Devices*, **ed-14**, 728 (1967); *ibid.*, **ed-15**, 951 (1968).
30. A. H. Agajanian, *IBM Tech. Rep.*, **22**, 1559 (1972).
31. E. A. Irene, *This Journal*, **121**, 1613 (1974); E. A. Irene and Y. J. van der Meulen, *ibid.*, **123**, 1380 (1976).
32. G. L. Vidale, "Measurements of the Absorption of Resonance Lines III, Vaporization of Sodium from Sodium Silicate Glasses," Generall Electric Co., Technical Information Series, R60SD390 (1960).
33. JANAF Thermochemical Tables, D. R. Stull and H. Prophet, Editors, Second ed., NSRDS-NBS 37 (1971).
34. N. J. Chou, C. M. Osburn, and Y. J. van der Meulen, *Appl. Phys. Lett.*, **22**, 380 (1973).
35. R. A. Bunghard, B. L. Gregory, C. W. Gwyn, and G. F. Derbenwick, "Process Dependence of Radiation Effects in CMOS Integrated Circuits," Final Report, AFWL Contract 75-198 (1975).
36. O. H. Krikorian, in "Proceedings of the Symposium on Engineering with Nuclear Explosives," Conf. 700101, Vol. 1, p. 481, Las Vegas, Nevada (1970).

Director
Armed Forces Radiobiology Research Institute
Defense Nuclear Agency
National Naval Medical Center
Bethesda, MD 20014
    ATTN Technical Library

Commander in Chief
U.S. European Command, JCS
APO New York 09128
    ATTN ECJ6-PF

Defense Communication Engineer Center
1860 Wiehle Avenue
Reston, VA 22090
    ATTN R410 James W. McLean
    ATTN R320 C. W. Bergman

Director
Defense Communications Agency
Washington, DC 20305
    ATTN 930 Monte I. Burgett, Jr.

Defense Documentation Center
Cameron Station
Alexandria, VA 22314
    ATTN TC

Director
Defense Intelligence Agency
Washington, DC 20301
    ATTN DS-4A2

Director
Defense Nuclear Agency
Washington, DC 20305
    ATTN STVL
    ATTN RAEV
    ATTN DDST
    ATTN TITL Tech Library

Commander
Field Command
Defense Nuclear Agency
Kirtland AFB, NM 87115
    ATTN FCPR

Director
Interservice Nuclear Weapons School
Kirtland AFB, NM 87115
    ATTN Document Control

Director
Joint Strat TGT Planning Staff JCS
Offutt AFB
Omaha, NE 68113
    ATTN JLTW-2

Chief
Livermore Division Fld Command DNA
Lawrence Livermore Laboratory
P.O. Box 808
Livermore, CA 94550
    ATTN FCPRL

Director
National Security Agency
Ft. George G. Meade, MD 20755
    ATTN Orland O. Van Gunten R-425
    ATTN TDL

OJCS/J-3
The Pentagon
Washington, DC 20301
    ATTN J-3 RDTA BR WWMCCS Plans Div

Under Secretary of Defense for Rsch & Engrg
Department of Defense
Washington, DC 20301
    ATTN S&SS (OS)

Project Manager
Army Tactical Data Systems
U.S. Army Electronics Command
Fort Monmouth, NJ 07703
    ATTN DRCPN-TDS-SD
    ATTN Dwaine B. Huewe

Commander
BMD System Command
P.O. Box 1500
Huntsville, AL 35807
    ATTN BDMSC-TEN

Commander
Frankford Arsenal
Bridge and Tacony Streets
Philadelphia, PA 19137
    ATTN SARFA-FCD

Commander
Harry Diamond Laboratories
2800 Powder Mill Road
Adelphi, MD 20783
    ATTN DRXDO-EM (2)
    ATTN DRXDO-NP
    ATTN DRXDO-RB
    ATTN DRXDO-TF
    ATTN DRXDO-RCC
    ATTN DRXDO-TI Tech Library
    ATTN J. McGarrity

Commanding Officer
Night Vision Laboratory
U.S. Army Electronics Command
Fort Belvoir, VA 22060
    ATTN Capt. Allan S. Parker

33

Commander
Picatinny Arsenal
Dover, NJ 07801
    ATTN SARPA-ND-C-E
    ATTN SMUPA-ND-N-E
    ATTN SMUPA-FR-S-P (2)
    ATTN SARPA-ND-N
    ATTN SMUPA-ND-D-B
    ATTN SMUPA-ND-W
    ATTN SARPA-FR-E

Commander
Redstone Scientific Information Center
U.S. Army Missile Command
Redstone Arsenal, AL 35809
    ATTN Chief, Documents

Secretary of the Army
Washington, DC 20310
    ATTN ODUSA or Daniel Willard

Director
TRASANA
White Sands Missile Range, NM 88002
    ATTN ATAA-EAC

Director
U.S. Army Ballistic Research Labs
Aberdeen Proving Ground, MD 21005
    ATTN DRXBR-X
    ATTN DRXBR-VL (2)
    ATTN DRXBR-AM
    ATTN DRXRD-BVL

Chief
U.S. Army Communications Sys. Agency
Fort Monmouth, NJ 07703
    ATTN SCCM-AD-SV Library

Commander
U.S. Army Electronics Command
Fort Monmouth, NJ 07703
    ATTN DRSEL-TL-IR
    ATTN DRSEL-CE-T
    ATTN DRSEL-CT-HDK
    ATTN DRSEL-GG-TD
    ATTN DRSEL-TL-MD
    ATTN DRSEL-TL-ND
    ATTN DRSEL-PL-ENV

Commander
U.S. Army Electronics Proving Ground
Fort Huachuca, AZ 85613
    ATTN STEEP-MT-M

Commandant
U.S. Army Engineer School
Fort Belvoir, VA 22060
    ATTN ATSE-CTD-CS

Commander-in-Chief
U.S. Army Europe and Seventh Army
APO New York 09403 (Heidelberg)
    ATTN ODCSE-E AEAGE-PI

Commandant
U.S. Army Field Artillery School
Fort Sill, OK 73503
    ATTN ATSFA-CTD-ME

Commander
U.S. Army Mat & Mechanics Rsch Center
Watertown, MA 02172
    ATTN DRXMR-HH

Commander
U.S. Army Materiel Dev. & Readiness Cmd.
5001 Eisenhower Avenue
Alexandria, VA 22333
    ATTN DRCDE-D

Commander
U.S. Army Missile Command
Redstone Arsenal, AL 35809
    ATTN DRSI-RGP
    ATTN DRCPM-PE-EA
    ATTN DRSMI-RGP
    ATTN DRSMI-TRA

Chief
U.S. Army Nuc. and Chemical Surety Group
Bldg. 2073, North Area
Fort Belvoir, VA 22060
    ATTN MOSG-ND

Commander
U.S. Army Nuclear Agency
7500 Backlick Road
Building 2073
Springfield, VA 22150
    ATTN ATCN-W

Commander
U.S. Army Tank Automotive Command
Warren, MI 48090
    ATTN DRCPM-GCM-SW

Commander
U.S. Army Test and Evaluation Command
Aberdeen Proving Ground, MD 21005
    ATTN DRSTE-EL
    ATTN DRSTE-NB

Commander
White Sands Missile Range
White Sands Missile Range, NM 88002
    ATTN STEWS-TE-NT

Chief of Naval Research
Navy Department
Arlington, VA 22217
    ATTN 427

Commanding Officer
Naval Avionics Facility
21st and Arlington Avenue
Indianapolis, IN 46218
    ATTN 942

Commander
Naval Electronic Systems Command
Naval Electronic Systems Cmd Hqs
Washington, DC 20360
    ATTN 504511
    ATTN 5032
    ATTN PME 117-21
    ATTN 50451
    ATTN ELEX 05323

Commanding Officer
Naval Intelligence Support Center
4301 Suitland Road, Bldg. 5
Washington, DC 20390
    ATTN NISC-45

Commander
Naval Ocean Systems Center
San Diego, CA 92152
    ATTN H. F. Wong

Director
Naval Research Laboratory
Washington, DC 20375
    ATTN 5210
    ATTN 5216
    ATTN 6631
    ATTN 6440
    ATTN 601 E. Wolicki
    ATTN 4104
    ATTN 7701
    ATTN 2627

Commander
Naval Sea Systems Command
Navy Department
Washington, DC 20362
    ATTN SEA-9931 (2)

Officer-in-Charge
Navay Surface Weapons Center
White Oak, Silver Spring, MD 20910
    ATTN WA501 Navy Nuc. Prgms Off.
    ATTN WA50
    ATTN WA52

Commander
Naval Surface Weapons Center
Dahlgren Laboratory
Dahlgren, VA 22448
    ATTN FUR Robert A. Amadori

Commander
Naval Weapons Center
China Lake, CA 93555
    ATTN 533 Tech Library

Commanding Officer
Naval Weapons Evaluation Facility
Kirtland AFB
Albuquerque, NM 87117
    ATTN ATG Mr. Stanley

Commanding Officer
Naval Weapons Support Center
Crane, IN 47522
    ATTN 70242
    ATTN 7024

Commanding Officer
Nuclear Weapons Tng. Center Pacitic
Naval Air Station, North Island
San Diego, CA 92135
    ATTN 50

Director
Strategic Systems Project Office
Navy Department
Washington, DC 20376
    ATTN NSP-27331
    ATTN NSP-2342
    ATTN SP 2701

AF Aero-Propulsion Laboratory, AFSC
Wright-Patterson AFB, OH 45433
    ATTN POD P. E. Stover

AF Geophysics Laboratory, AFSC
Hanscom AFB, MA 01731
    ATTN LQR Edward A. Burke
    ATTN J. Emery Cormier
    ATTN LGD-Stop 30 Freeman Shepherd

AF Institute of Technology, AU
Wright-Patterson AFB, OH 45433
    ATTN ENP Charles J. Bridgman

AF Materials Laboratory, AFSC
Wright-Patterson AFB, OH 45433
    ATTN LTE

AF Weapons Laboratory, AFSC
Kirtland AFB, NM 87117
    ATTN DEX
    ATTN ELA
    ATTN NTS
    ATTN ELP Tree Section
    ATTN NT Carl E. Baum
    ATTN ELS
    ATTN ELXT

AFTAC
Patrick AFB, FL 32925
    ATTN TAE
    ATTN TFS Maj. Marion F. Schneider

Air Force Avionics Laboratory, AFSC
Wright-Patterson AFB, OH 45433
    ATTN AAT Mason Friar
    ATTN DHM C. Friend
    ATTN DH LtC. McKenzie
    ATTN DHE H. J. Hennecke

Commander
ASD
Wright-Patterson AFB, OH 45433
    ATTN ASD/ENESS
    ATTN ASD-YH-EX
    ATTN ENACC Robert L. Fish

Headquarters
Electronic Systems Division/YS
Hanscom AFB, MA 01731
    ATTN YSEV

Headquarters
Electronic Systems Division/YW
Hanscom AFB, MA 01731
    ATTN YWEI

Commander
Foreign Technology Division, AFSC
Wright-Patterson AFB, OH 45433
    ATTN ETD/PDJC
    ATTN ETDP

Commander
Ogden Air Logistics Center
Hill AFB, UT 84401
    ATTN MMEWM

Commander
Rome Air Development Center, AFSC
Griffiss AFB, NY 13440
    ATTN RBRAC
    ATTN RBRP

Commander
Rome Air Development Center, AFSC
Hanscom AFB, MA 01731
    ATTN ETS
    ATTN ET R. Buchanan

SAMSO/DY
P.O. Box 92960
Worldway Postal Center
Los Angeles, CA 90009
    ATTN DYS

SAMSO/IN
P.O. Box 92960
Worldway Postal Center
Los Angeles, CA 90009
    ATTN IND I. J. Judy

SAMSO/MN
Norton AFB, CA 92409
    ATTN MNNH

SAMSO/RS
P.O. Box 92960
Worldway Postal Center
Los Angeles, CA 90009
    ATTN RSSE
    ATTN RSMG

SAMSO/SK
P.O. Box 92960
Worldway Postal Center
Los Angeles, CA 90009
    ATTN SKF

SAMSO/SZ
P.O. Box 92960
Worldway Postal Center
Los Angeles, CA 90009
    ATTN SZJ

Commander in Chief
Strategic Air Command
Offutt AFB, NB 68113
    ATTN NRI-STINFO Library
    ATTN XPFS

Department of Energy
Albuquerque Operations Office
P.O. Box 5400
Albuquerque, NM 87115
    ATTN Document Control for WSSB

University of California
Lawrence Livermore Laboratory
P.O. Box 808
Livermore CA   94550
    ATTN Lawrence Cleland L-156
    ATTN E. K. Miller L-156
    ATTN Frederick R. Kovar L-31 (Class L-94)
    ATTN Joseph E. Keller, Jr. L-125
    ATTN Hans Kruger L-96 (Class L-94)
    ATTN Tech. Info. Dept. L-3
    ATTN Ronald L. Ott L-531
    ATTN William J. Hogan L-389
    ATTN Donald J. Meeker L-545 (Class L-153)

Los Alamos Scientific Laboratory
P.O. Box 1663
Los Alamos, NM   87545
    ATTN DOC CON for J. Arthur Freed
    ATTN DOC CON for Bruce W. Noel

Sandia Laboratories
P.O. Box 5800
Albuquerque, NM   87115
    ATTN DOC CON for R. Gregory ORG 2140
    ATTN DOC CON for 3141 Sandia Rpt Coll
    ATTN DOC CON for J. A. Hood ORG 2110

Department of Commerce
National Bureau of Standards
Washington, DC   20234
    ATTN Judson C. French

Aerojet Electro-Systems Co.
Div. of Aerojet-General Corporation
P.O. Box 296, 1100 W. Hollyvale Drive
Azusa, CA   91702
    ATTN Thomas D. Hanscome

Aerospace Corporation
P.O. Box 92957
Los Angeles, CA   90009
    ATTN John Ditre
    ATTN Irving M. Garfunkel
    ATTN S. P. Bower
    ATTN Library
    ATTN L. W. Aukerman
    ATTN Julian Reinheimer
    ATTN William W. Willis

Analog Technology Corporation
3410 East Foothill Boulevard
Pasadena, CA   91107
    ATTN John Joseph Baum

AVCO Research & Systems Group
201 Lowell Street
Wilmington, MA   01887
    ATTN Research Lib. A830 Rm 7201

BDM Corporation, The
7915 Jones Branch Drive
McLean, VA   22101
    ATTN T. H. Neighbors

BDM Corporation, The
P.O. Box 9274
Albuquerque International
Albuquerque, NM   87119
    ATTN D. R. Alexander

Bendix Corporation, The
Communication Division
East Joppa Road
Baltimore, MD   21204
    ATTN Document Control

Bendix Corporation, The
Research Laboratories Division
Bendix Center
Southfield, MI   48075
    ATTN Mgr Prgm Dev Donald J. Niehaus
    ATTN Max Frank

Boeing Company, The
P.O. Box 3707
Seattle, WA   98124
    ATTN Howard W. Wicklein MS 17-11
    ATTN Aerospace Library
    ATTN Donald W. Egelkrout MS 2R-00
    ATTN Itsu Amura
    ATTN Robert S. Caldwell 2R-00
    ATTN Carl Rosenberg 2R-00

Booz-Allen and Hamilton, Inc.
106 Apple Street
Tinton Falls, NJ   07724
    ATTN Raymond J. Chrisner

California Institute of Technology
Jet Propulsion Laboratory
4800 Oak Grove Drive
Pasadena, CA   91103
    ATTN J. Bryden
    ATTN A. G. Stanley

Charles Stark Draper Laboratory, Inc.
555 Technology Square
Cambridge, MA   02139
    ATTN Paul R. Kelly
    ATTN Kenneth Fertig

Cincinnati Electronics Corporation
2630 Glendale-Milford Road
Cincinnati, OH   45241
    ATTN C. R. Stump
    ATTN Lois Hammond

Control Data Corporation
P.O. Box 0
Minneapolis, MN 55440
    ATTN Jack Meehan

Cutler-Hammer, Inc.
AIL Division
Comack Road
Deer Park, NY 11729
    ATTN Central Tech Files Anne Anthony

Denver, University of
Colorado Seminary
Denver Research Institute
P.O. Box 10127
Denver, CO 80210
    ATTN Sec. Officer for Fred P. Venditti

Dikewood Industries, Inc.
1009 Bradbury Drive, S.E.
Albuquerque, NM 87106
    ATTN L. Wayne Davis

E-Systems, Inc.
Greenville Division
P.O. Box 1056
Greenville, TX 75401
    ATTN Library 8-50100

Effects Technology, Inc.
5383 Hollister Avenue
Santa Barbara, CA 93111
    ATTN Edward John Steele

Exp & Math Physics Consultants
P.O. Box 66331
Los Angeles, CA 90066
    ATTN Thomas M. Jordan

Fairchild Camera and Instrument Corp
464 Ellis Street
Mountain View, CA 94040
    ATTN Sec. Dept for 2-233 David K. Myers

Fairchild Industries, Inc.
Sherman Fairchild Technology Center
20301 Century Boulevard
Germantown, MD 20767
    ATTN Mgr Config Data & Standards

Florida, University of
An Institution of Education
ATTN: Patricia B. Rambo
P.O. Box 284
Gainesville, FL 32601
    ATTN D. P. Kennedy

Ford Aerospace & Communications Corp.
3939 Fabian Way
Palo Alto, CA 94303
    ATTN Edward R. Hahn MS-X22
    ATTN Donald R. McMorrow MS G30
    ATTN Samuel R. Crawford MS 531

Ford Aerospace & Communications Operations
Ford & Jamboree Roads
Newport Beach, CA 92663
    ATTN Ken C. Attinger
    ATTN E. R. Poncelet, Jr.
    ATTN Tech Info Section

Franklin Institute, The
20th Street and Parkway
Philadelphia, PA 19103
    ATTN Ramie H. Thompson

Garrett Corporation
P.O. Box 92248, 9851 Sepulveda Blvd.
Los Angeles, CA 90009
    ATTN Robert E. Weir Dept 93-9

General Dynamics Corp.
Electronics Div. Orlando Operations
P.O. Box 2566
Orlando, FL 32802
    ATTN D. W. Coleman

General Electric Company
Space Division
Valley Forge Space Center
Goddard Blvd, King of Prussia
P.O. Box 8555
Philadelphia, PA 19101
    ATTN John L. Andrews
    ATTN Joseph C. Peden VFSC. Rm 4230M
    ATTN Larry I. Chasen

General Electric Company
Re-entry & Environmental Systems Div
P.O. Box 7722
3198 Chestnut Street
Philadelphia, PA 19101
    ATTN Robert V. Benedict
    ATTN John W. Palchefsky, Jr.

General Electric Company
Ordnance Systems
100 Plastics Avenue
Pittsfield, MA 01201
    ATTN Joseph J. Reidl

General Electric Company
Tempo-Center for Advanced Studies
816 State Street (P.O. Drawer QQ)
Santa Barbara, CA 93102
    ATTN William McNamera
    ATTN M. Espig
    ATTN Royden R. Rutherford
    ATTN DASIAC

General Electric Company
Aircraft Engine Business Group
Evendale Plant Int Hwy 75 S
Cincinnati, OH 45215
    ATTN John A. Ellerhorst E 2

General Electric Company
Aerospace Electronics Systems
French Road
Utica, NY 13503
    ATTN W. J. Patterson Drop 233
    ATTN Charles M. Hewison Drop 624

General Electric Company
P.O. Box 5000
Binghamton, NY 13902
    ATTN David W. Pepin Drop 160

General Electric Company-Tempo
ATTN: DASIAC
c/o Defense Nuclear Agency
Washington, DC 20305
    ATTN William Alfonte

General Research Corporation
P.O. Box 3587
Santa Barbara, CA 93105
    ATTN Robert D. Hill

Georgia Institute of Technology
Georgia Tech Research Institute
Atlanta, GA 30332
    ATTN R. Curry (uncl only)

Grumman Aerospace Corporation
South Oyster Bay Road
Bethpage, NY 11714
    ATTN Jerry Rogers Dept 533

GTE Sylvania, Inc.
Electronics Systems Grp-Eastern Div
77 A Street
Needham, MA 02194
    ATTN James A. Waldon
    ATTN Charles A. Thornhill Librarian
    ATTN Leonard L. Blaisdell

GTE Sylvania, Inc.
189 B Street
Needham Heights, MA 02194
    ATTN H & V Group
    ATTN Paul B. Frederickson
    ATTN Herbert A. Ullman
    ATTN Charles H. Ramsbottom

Gulton Industries, Inc.
Engineered Magnetics Division
13041 Cerise Avenue
Hawthorne, CA 90250
    ATTN Engnmagnetics Div

Harris Corporation
Harris Semiconductor Division
P.O. Box 883
Melbourne, FL 32901
    ATTN Carl F. Davis MS 17-220
    ATTN Wayne E. Abare MS 16-111
    ATTN T. L. Clark MS 4040

Hazeltine Corporation
Pulaski Road
Greenlawn, NY 11740
    ATTN Tech Info Ctr M. Waite

Honeywell Incorporated
Avionics Division
2600 Ridgeway Parkway
Minneapolis, MN 55413
    ATTN Ronald R. Johnson A1622
    ATTN R. J. Kell MS S2572

Honeywell Incorporated
Avionics Division
13350 U.S. Highway 19 North
St. Petersburg, FL 33733
    ATTN Harrison H. Noble MS 725-5A
    ATTN Stacey H. Graff MS 725-5

Honeywell Incorporated
Radiation Center
2 Forbes Road
Lexington, MA 02173
    ATTN Technical Library

Hughes Aircraft Company
Centinela and Teale
Culver City, CA 90230
    ATTN John B. Singletary MS 6-D133
    ATTN Dan Binder MS 6-D147
    ATTN Kenneth R. Walker MS D157
    ATTN Billy W. Campbell MS 6-E110

Hughes Aircraft Company, El Segundo Site
P.O. Box 92919
Los Angeles, CA 90009
    ATTN Edward C. Smith MS A620
    ATTN William W. Scott MS A1080

IBM Corporation
Route 17C
Owego, NY 13827
    ATTN Harry W. Mathers Dept M41
    ATTN Frank Frankovsky

IIT Research Institute
10 West 35th Street
Chicago, IL 60616
    ATTN Irving N. Mindel

Intl. Tel. & Telegraph Corporation
500 Washington Avenue
Nutley, NJ 07110
    ATTN Alexander T. Richardson

Ion Physics Corporation
South Bedford Street
Burlington, MA 01803
    ATTN Robert D. Evans

IRT Corporation
P.O. Box 81087
San Diego, CA 92138
    ATTN Leo D. Cotter
    ATTN MDC
    ATTN R. L. Mertz

JAYCOR
1401 Camino Del Mar
Del Mar, CA 92014
    ATTN Eric P. Wenaas

JAYCOR
205 S. Whiting Street, Suite 500
Alexandria, VA 22304
    ATTN Robert Sullivan
    ATTN Catherine Turesko

Johns Hopkins University
Applied Physics Laboratory
Johns Hopkins Road
Laurel, MD 20810
    ATTN Peter E. Partridge

Kaman Sciences Corporation
P.O. Box 7463
Colorado Springs, CO 80933
    ATTN Donald H. Bryce
    ATTN Albert P. Bridges
    ATTN John R. Hoffman
    ATTN Jerry I. Lubell
    ATTN W. Foster Rich
    ATTN Walter E. Ware

Litton Systems, Inc.
Guidance & Control Systems Division
5500 Canoga Avenue
Woodland Hills, CA 91364
    ATTN Val J. Ashby MS 67
    ATTN John P. Retzler
    ATTN R. W. Maughmer

Litton Systems, Inc.
Electron Tube Division
1035 Westminster Drive
Williamsport, PA 17701
    ATTN Frank J. McCarthy

Lockheed Missiles & Space Co., Inc.
P.O. Box 504
Sunnyvale, CA 94088
    ATTN Samuel I. Taimuty, Dept 85-85
    ATTN L. Rossi, Dept 81-64
    ATTN Benjamin T. Kimura, Dept.81-14
    ATTN Edwin A. Smith, Dept 85-85
    ATTN George F. Heath, Dept 81-14

Lockheed Missiles and Space Co., Inc.
3251 Hanover Street
Palo Alto, CA 94304
    ATTN Tech Info Ctr D/Coll

M.I.T. Lincoln Laboratory
P.O. Box 73
Lexington, MA 02173
    ATTN Leona Loughlin Librarian A-082

Martin Marietta Corporation
Orlando Division
P.O. Box 5837
Orlando, FL 32805
    ATTN Mona C. Griffith Lib MP-30
    ATTN William W. Mras MP-413
    ATTN Jack M. Ashford MP-537

Martin Marietta Corporation
Denver Division
P.O. Box 179
Denver, CO 80201
    ATTN Ben T. Graham MS PO-454
    ATTN Research Lib 6617 Jay R. McKee
    ATTN J. E. Goodwin Mail 0452
    ATTN Paul G. Kase Mail 8203

McDonnell Douglas Corporation
P.O. Box 516
St. Louis, Missouri 63166
    ATTN Tom Ender
    ATTN Technical Library

McDonnell Douglas Corporation
5301 Bolsa Avenue
Huntington Beach, CA 92647
    ATTN Stanley Schneider

McDonnell Douglas Corporation
3855 Lakewood Boulevard
Long Beach, CA 90846
    ATTN Technical Library, Cl-290/36-84

Mission Research Corporation
735 State Street
Santa Barbara, CA 93101
    ATTN William C. Hart

Mission Research Corporation
P.O. Box 8693, Station C
Albuquerque, NM 87108
    ATTN David E. Merewether

Mission Research Corporation - San Diego
P.O. Box 1209
La Jolla, CA 92038
    ATTN J. P. Raymond
    ATTN V. A. J. Van Lint

Mitre Corporation, The
P.O. Box 208
Bedford, MA 01730
    ATTN M. E. Fitzgerald
    ATTN Library

National Academy of Sciences
ATTN: National Materials Advisory Board
2101 Constitution Avenue, NW
Washington, DC 20418
    ATTN R. S. Shane Nat Materials Advsy

New Mexico, University of
Electrical Engineering & Computer Science Dept
Albuquerque, NM 87131
    ATTN Harold Southward

Northrop Corporation
Electronic Division
1 Research Park
Palos Verdes Peninsula, CA 90274
    ATTN George H. Towner
    ATTN Boyce T. Ahlport

Northrop Corporation
Northrop Research and Technology Ctr
3401 West Broadway
Hawthorne, CA 90250
    ATTN Orlie L. Curtis, Jr.
    ATTN J. R. Srour
    ATTN David N. Pocock

Northrop Corporation
Electronic Division
2301 West 120th Street
Hawthorne, CA 90250
    ATTN Joseph D. Russo
    ATTN John M. Reynolds
    ATTN Vincent R. DeMartino

Palisades Inst for Research Services, Inc.
201 Varick Street
New York, NY 10014
    ATTN Records Supervisor

Physics International Company
2700 Merced Street
San Leandro, CA 94577
    ATTN Doc Con for Charles H. Stallings
    ATTN Doc Con for John H. Huntington

R & D Associates
P.O. Box 9695
Marina Del Rey, CA 90291
    ATTN S. Clay Rogers

Rand Corporation, The
1700 Main Street
Santa Monica, CA 90406
    ATTN Cullen Crain

Raytheon Company
Hartwell Road
Bedford, MA 01730
    ATTN Gajanan H. Joshi Radar Sys Lab

Raytheon Company
528 Boston Post Road
Sudbury, MA 01776
    ATTN Harold L. Flescher

RCA Corporation
Government Systems Division
Astro Electronics
P.O. Box 800, Locust Corner
East Windsor Township
Princeton, NJ 08540
    ATTN George J. Brucker

RCA Corporation
Camden Complex
Front & Cooper Streets
Camden, NJ 08012
    ATTN E. Van Keuren 13-5-2

Rensselaer Polytechnic Institute
P.O. Box 965
Troy, NJ 12181
    ATTN Ronald J. Gutmann

Research Triangle Institute
P.O. Box 12194
Research Triangle Park, NC 27709
     ATTN Sec Officer for
     ATTN Eng Div Mayrant Simons, Jr.

Rockwell International Corporation
P.O. Box 3105
Anaheim, CA 92803
     ATTN George C. Messenger FB61
     ATTN Donald J. Stevens FA70
     ATTN K. F. Hull
     ATTN James E. Bell HA10
     ATTN N. J. Rudie FA53

Rockwell International Corporation
5701 West Imperial Highway
Los Angeles, CA 90009
     ATTN T. B. Yates

Rockwell International Corporation
Collins Divisions
400 Collins Road NE
Cedar Rapids, IA 52406
     ATTN Mildred A. Blair
     ATTN Dennis Sutherland
     ATTN Alan A. Langenfeld

Sanders Associates, Inc.
95 Canal Street
Nashua, NH 03060
     ATTN Moe L. Aitel NCA 1-3236

Science Applications, Inc.
P.O. Box 277
Berkeley, CA 94701
     ATTN Frederick M. Tesche

Science Applications, Inc.
P.O. Box 2351
La Jolla, CA 92038
     ATTN J. Robert Beyster
     ATTN Larry Scott

Science Applications, Inc.
Huntsville Division
2109 W. Clinton Avenue
Suite 700
Huntsville, AL 35805
     ATTN Noel R. Byrn

Science Applications, Inc.
P.O. Box 3507
Albuquerque, NM 87110
     ATTN J. Roger Hill

Science Applications, Inc.
8400 Westpark Drive
McLean, VA 22101
     ATTN William L. Chadsey

Singer Company (Data Systems), The
150 Totowa Road
Wayne, NJ 07470
     ATTN Tech Info Center

Singer Company, The
ATTN: Security Manager
1150 McBride Avenue
Little Falls, NJ 07424
     ATTN Irwin Goldman Eng Management

Sperry Flight Systems Division
Sperry Rand Corporation
P.O. Box 21111
Phoenix, AZ 85036
     ATTN D. Andrew Schow

Sperry Rand Corporation
Sperry Division
Marcus Avenue
Great Neck, NY 11020
     ATTN Charles L. Craig EV
     ATTN Paul Maraffino

Sperry Univac
Univac Park, P.O. Box 3525
St. Paul, MN 55165
     ATTN James A. Inda MS 41T25

SRI International
333 Ravenswood Avenue
Menlo Park, CA 94025
     ATTN Philip J. Dolan
     ATTN Arthur Lee Whitson

SRI International
306 Wynn Drive, NW
Huntsville, AL 35805
     ATTN MacPherson Morgan

Sundstrand Corporation
4751 Harrison Avenue
Rockford, IL 61101
     ATTN Curtis B. White

Systron-Donner Corporation
1090 San Miguel Road
Concord, CA 94518
     ATTN Gordon B. Dean
     ATTN Harold D. Morris

Texas Instruments, Inc.
P.O. Box 5474
Dallas, TX 75222
     ATTN Donald J. Manus MS 72

Texas Tech University
P.O. Box 5404 North College Station
Lubbock, TX 79417
     ATTN Travis L. Simpson

42

TRW Defense & Space Sys Group
One Space Park
Redondo Beach, CA 90278
    ATTN O. E. Adams R1-1144
    ATTN H. H. Holloway R1-2036
    ATTN Tech Info Center/S-1930
    ATTN R. K. Plebuch R1-2078
    ATTN Robert M. Webb R1-2410

TRW Defense & Space Sys Group
San Bernardino Operations
P.O. Box 1310
San Bernardino, CA 92402
    ATTN F. B. Fay
    ATTN R. Kitter

United Technologies Corporation
Hamilton Standard Division
Bradley International Airport
Windsor Locks, CT 06069
    ATTN Raymond G. Giguere

Vought Corporation
P.O. Box 5907
Dallas, TX 75222
    ATTN Technical Data Ctr

Westinghouse Electric Corporation
Defense and Electronic Systems Ctr
P.O. Box 1693
Baltimore-Washington Intl Airport
Baltimore, MD 21203
    ATTN Henry P. Kalapaca MS 3525

U.S. DEPT. OF COMM. BIBLIOGRAPHIC DATA SHEET	1. PUBLICATION OR REPORT NO. NBSIR 77-1404	2. Gov't Accession No.	3. Recipient's Accession No.
4. TITLE AND SUBTITLE Control of Mobile-Ion Contamination in Oxidation Ambients for MOS Device Processing			5. Publication Date January 1978
			6. Performing Organization Code
7. AUTHOR(S) Santos Mayo, Richard Y. Koyama, and Thomas F. Leedy			8. Performing Organ. Report No. NBSIR -77-1404
9. PERFORMING ORGANIZATION NAME AND ADDRESS NATIONAL BUREAU OF STANDARDS DEPARTMENT OF COMMERCE WASHINGTON, D.C. 20234			10. Project/Task/Work Unit No. Z99QAXTD072 W.U. 66
			11. Contract/Grant No. DNA IACRO 77-809
12. Sponsoring Organization Name and Complete Address (Street, City, State, ZIP) Defense Nuclear Agency Washington, D. C. 20305			13. Type of Report & Period Covered Final Oct. 1976-Oct. 1977
			14. Sponsoring Agency Code

15. SUPPLEMENTARY NOTES

16. ABSTRACT *(A 200-word or less factual summary of most significant information. If document includes a significant bibliography or literature survey, mention it here.)*

An alternative method for controlling the mobile-ion contamination in the oxidation ambients for MOS device processing is explored. Mobile-ion contamination in silicon dioxide films thermally grown in dry oxygen at 1000°C on silicon substrates has been studied by use of a double-wall fused-silica oxidation tube. The space between the tubes were alternatively filled with chlorine, room air, or sodium hydroxide gas to determine if a correlation exists between the presence of these substances in the jacket and the mobile-ion density in the oxide films. MOS capacitors were prepared on these films and mobile-ion densities were measured using conventional C-V techniques. The ion densities ranged from 10^{13} to 10^{10} cm^{-2} as a function of the jacket atmosphere. These preliminary results suggest that there is a correlation between the presence of cleaning or contaminating agents in the jacket and the mobile-ion density in the oxide films. Both cleaning and contaminating actions occur through the tube wall.

17. KEY WORDS *(six to twelve entries; alphabetical order; capitalize only the first letter of the first key word unless a proper name; separated by semicolons)*

Double-wall oxidation tube; dry oxidation; mobile-ion contamination; MOS device processing; MOS devices; oxidation ambient control; oxide growth; semiconductor device processing; silicon dioxide; thermal silicon dioxide films.

18. AVAILABILITY ☒ Unlimited	19. SECURITY CLASS (THIS REPORT)	21. NO. OF PAGES
☐ For Official Distribution. Do Not Release to NTIS	UNCLASSIFIED	43
☐ Order From Sup. of Doc., U.S. Government Printing Office Washington, D.C. 20402, SD Cat. No. C13	20. SECURITY CLASS (THIS PAGE)	22. Price
☒ Order From National Technical Information Service (NTIS) Springfield, Virginia 22151	UNCLASSIFIED	$4.50